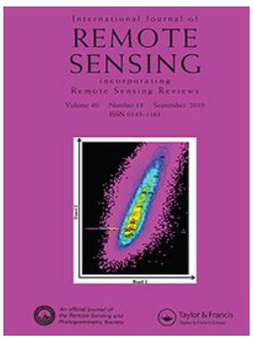

International Journal of Remote Sensing

ISSN: 0143-1161 (Print) 1366-5901 (Online) Journal homepage: https://www.tandfonline.com/loi/tres20

A random forest-based framework for crop mapping using temporal, spectral, textural and polarimetric observations

Iman Khosravi & Seyed Kazem Alavipanah

To cite this article: Iman Khosravi & Seyed Kazem Alavipanah (2019) A random forest-based framework for crop mapping using temporal, spectral, textural and polarimetric observations, International Journal of Remote Sensing, 40:18, 7221-7251, DOI: 10.1080/01431161.2019.1601285

To link to this article: https://doi.org/10.1080/01431161.2019.1601285

INTERNATIONAL JOURNAL OF REMOTE SENSING
2019, VOL. 40, NO. 18, 7221–7251
https://doi.org/10.1080/01431161.2019.1601285

Taylor & Francis
Taylor & Francis Group

A random forest-based framework for crop mapping using temporal, spectral, textural and polarimetric observations

Iman Khosravi and Seyed Kazem Alavipanah

Department of Remote Sensing and GIS, Faculty of Geography, University of Tehran, Tehran, I.R. Iran

ABSTRACT

Combining optical and polarimetric synthetic aperture radar (PolSAR) earth observations offers a complementary data set with a significant number of spectral, textural, and polarimetric features for crop mapping and monitoring. Moreover, a temporal combination of both sources of information may lead to obtaining more reliable results compared to the use of single-time observations. In this paper, an operational framework based on the stacked generalization of random forest (RF), which efficiently employed bi-temporal observations of optical and radar data, was proposed for crop mapping. In the first step, various spectral, vegetation index, textural, and polarimetric features were extracted from both data sources and placed into several groups. Each group was classified separately using a single RF classifier. Then, several additional classification tasks were accomplished by another RF classifier. The earth observations used in this paper were collected by RapidEye satellites and the Unmanned Aerial Vehicle Synthetic Aperture Radar (UAVSAR) system over an agricultural region near Winnipeg, Manitoba, Canada. The results confirmed that the proposed methodology was able to provide a higher overall accuracy and kappa coefficient than traditional stacking method, and also than all the individual RFs using each group. These accuracy metrics were also better than those of the RFs using the stacked features. Moreover, only the proposed methodology could achieve standard accuracy (*F*-score ≥85%) for all crop types in the study area. The visual comparison also demonstrated that the crop maps produced by the proposed methodology had more homogeneous, uniform appearances. Moreover, the mixed pixels of crop types, which abundantly existed in the traditional stacking and individual RFs' maps, were significantly eliminated.

ARTICLE HISTORY
Received 2 October 2018
Accepted 23 January 2019

1. Introduction

Crop mapping is an essential need in agriculture planning and management activities at national and global scales. A reliable crop map plays an important role with regard to various applications in environmental and agricultural management, such as crop inventory, crop insurance, yield estimation and the enforcement of quota limits (Zhu, Radeloff, and Ives

CONTACT Iman Khosravi iman.khosravi@ut.ac.ir Department of Remote Sensing and GIS, Faculty of Geography, University of Tehran, Tehran, I.R. Iran

This article was originally published with errors, which have now been corrected in the online version. Please see Correction (http://dx.doi.org/10.1080/01431161.2019.1613058)

2017). Remote sensing and earth observation technologies exhibit valuable optical and radar sensors, offering various spatial and temporal resolutions. These sensors can be used for crop mapping and monitoring in a more efficient manner and with lower costs than traditional survey methods (Villa et al. 2015).

To date, optical satellites, such as Moderate Resolution Imaging Spectroradio-meter (MODIS), Landsat, National Oceanic and Atmospheric Administration (NOAA), Indian Remote Sensing (IRS), and Satellite Pour l'Observation de la Terre (SPOT), have extensively been utilized in crop mapping studies at global, national, regional and local scales (e.g. Wardlow and Egbert 2010; Pittman et al. 2010; Chen et al. 2011; Vintrou et al. 2012; Zheng, Campbell, and de Beurs 2012; Son et al., 2014; You et al. 2013; Esch et al. 2014; You, Pei, and Wang 2014; Jin et al. 2015; Peña and Brenning 2015; Schultz et al. 2015; Zheng et al. 2015; Eisavi, Homayouni, and Rezaei-Chiyaneh 2017; Sonobe et al. 2017). In recent years, RapidEye (e.g., Löw et al. 2012; Kim and Yeom 2014; Siachalou, Mallinis, and Tsakiri-Strati 2015; Kross et al. 2015) and Sentinel-2 (e.g., Immitzer, Vuolo, and Atzberger 2016; Clevers, Kooistra, and van Den Brande 2017; Ng et al. 2017; Song et al. 2017; Zheng et al. 2017; Belgiu and Csillik, 2018) have also been of interest to researchers for crop mapping and monitoring. Compared to the aforementioned optical sensors, these two satellites have a unique spectral band for analyzing vegetation, known as the red edge (RE). Moreover, thanks to the simultaneous orbiting of five RapidEye sensors, it can frequently acquire images from a given area. These two advantages have distinguished RapidEye from the other optical satellite systems for agricultural applications (Schuster, Förster, and Kleinschmit 2012).

The primary observations of optical sensors for crop mapping are in the form of multispectral information in the range of visible to near-infrared (NIR) wavelengths, which characterize the reflectance behaviour of crop types (Joshi et al. 2016). However, vegetation indices (VIs), mainly based on red and NIR bands, are the most widely used products of optical sensors, providing more valuable information for discriminating various crop types. The normalized difference vegetation index (NDVI), simple ratio (SR) and enhanced vegetation index (EVI) are the most well-known VIs according to previous crop mapping studies (Peña-Barragán et al. 2011; Chellasamy, Zielinski, and Greve 2014). Moreover, some applicable VIs based on RE channels, such as the red-edge NDVI (NDVIre), red-edge SR (SRre) and red-edge triangular vegetation index (RTVIcore), were recently proposed and used in the literature (Kross et al. 2015). In addition to the spectral bands and VIs, textural indicators have proven to be useful features for crop mapping (Peña-Barragán et al. 2011; Ursani et al. 2012). The most well-known textural features already used for crop mapping are the parameters extracted from the grey level co-occurrence matrix (GLCM) of spectral channels (Kim and Yeom 2014). These features describe the spatial arrangement of grey levels in an image (Gonzalez and Woods 2002).

Compared to the optical sensors, fewer studies have so far employed synthetic aperture radar (SAR) or full-polarimetric SAR (PolSAR) sensors, such as the European Remote Sensing (ERS), the Advanced Synthetic Aperture Radar (ASAR) and Radarsat, for crop mapping on regional or local scales (McNairn et al. 2009b; Bouvet and Le Toan 2011; Qi et al. 2012; Brisco et al. 2013; Liu et al. 2013; Niu and Ban 2013; Jiao et al. 2014; Hoang et al. 2016; Canisius et al. 2018). The Unmanned Aerial Vehicle Synthetic Aperture Radar (UAVSAR) system, as an airborne PolSAR sensor, has been recently used in several

studies for agricultural applications, thanks to its tolerable revisit time (e.g., Hosseini et al. 2015; Khosravi et al. 2017; Tamiminia et al. 2017; Whelen and Siqueira 2017).

The primary observations of single-polarized SAR sensors are in the form of complex polarization data, i.e., a backscattered signal's intensity and phase, which contain essential information about the physical and geometrical nature of vegetation and crops (Panigrahy et al. 2012). Furthermore, a wider variety of parameters, such as polarimetric variables and target decompositions, which are relevant to the scattering mechanisms of different surface objects and land covers, can be extracted from PolSAR data. Many studies have already reported advantages regarding the polarimetric features extracted from PolSAR data, compared to single and multipolarization data for crop mapping (e.g., Lardeux et al. 2009; Larrañaga and Álvarez-Mozos 2016; Hoang et al. 2016; Tamiminia et al. 2017).

In the past two decades, several researchers have used the combination or fusion of optical and radar images for crop mapping and monitoring (Waske and Benediktsson 2007; Waske and van der Linden 2008; McNairn et al. 2009a; Larrañaga, Álvarez-Mozos, and Albizua 2011; Torbick et al. 2011; Haldar et al. 2012; Forkuor et al. 2014; Villa et al. 2015; Zhang, Lin, and Li 2015; Hütt et al. 2016; Inglada et al. 2016; Joshi et al. 2016; Kussul et al. 2016; Navarro et al. 2016; Skakun et al. 2016; Wang et al. 2016; Ferrant et al. 2017; Mansaray et al. 2017; Qiao, Daneshfar, and Davidson 2017; Torbick et al. 2017; Salehi, Daneshfar, and Davidson 2017; Zhou et al. 2017; Steinhausen et al. 2018; Van Tricht et al. 2018; Denize et al. 2019). The joint use of optical and radar data has two advantages. Firstly, it helps to alleviate their specific limitations, i.e., dependency on weather and atmospheric conditions in optical images and speckle defects in radar images. Secondly, it takes advantage of their complementarity regarding sensitivity to vegetation and soil characteristics (Villa et al. 2015). On the other hand, characteristics of crops and their phenologies change during the growing season. Many studies have shown that the temporal combination of optical and SAR observations can often lead to more reliable and efficient results for crop mapping (e.g., Torbick et al. 2011; Villa et al. 2015; Inglada et al. 2016; Kussul et al. 2016; Skakun et al. 2016). Accordingly, this combination could generate a full and big optic radar data set with an exhaustive temporal, spectral, textural and polarimetric feature space for crop mapping. Nonetheless, research that has utilized and examined the capability and effectiveness of various optical and radar features together is limited.

Diverse classification algorithms with a different nature and architecture have already been proposed for crop mapping. Some studies have used Bayesian networks or the maximum likelihood method (e.g., Larrañaga, Álvarez-Mozos, and Albizua 2011; Haldar et al. 2012; Hütt et al. 2016; Qiao, Daneshfar, and Davidson 2017; Salehi, Daneshfar, and Davidson 2017). These two traditional methods are parametric, i.e., they strongly depend on data distribution. Therefore, they may be limited in the classification of big data. Some other studies have used nonparametric methods, such as neural networks, support vector machines (SVM), or both (e.g., Waske and van der Linden 2008; McNairn et al. 2009a; Kussul et al. 2016; Navarro et al. 2016; Skakun et al. 2016; Wang et al. 2016; Denize et al. 2019). A neural network, which has a black box architecture, is known as an unstable classifier in the literature (Cunningham, Carney, and Jacob 2000; Polikar 2006; Du et al. 2012). By contrast, an SVM is known as an efficient and stable method for the classification of high-dimensional data in the literature. However, there are some major challenges for SVMs, such as the choice of optimum kernels and their parameters, and

the effect of noise or outliers in data on SVM performance (Mountrakis, Im, and Ogole 2011). Other nonparametric algorithms used for crop mapping are tree-based classifiers, such as decision trees and random forest (RF) (e.g., Waske and van der Linden 2008; McNairn et al. 2009a; Torbick et al. 2011; Forkuor et al. 2014; Villa et al. 2015; Hütt et al. 2016; Inglada et al. 2016; Wang et al. 2016; Ferrant et al. 2017; Mansaray et al. 2017; Qiao, Daneshfar, and Davidson 2017; Torbick et al. 2017; Salehi, Daneshfar, and Davidson 2017; Steinhausen et al. 2018; Van Tricht et al. 2018; Denize et al. 2019). A decision tree is a weak classifier (Breiman 1996; Du et al. 2012) and may be faced with limitations in the classification of big data. Conversely, an RF, whose construction is based on a multitude of decision trees, has a high level of capability in this condition, which is comparable to an SVM. Moreover, an RF is preferred over an SVM thanks to its various advantages: an RF is much faster, more flexible and more robust in relation to the outliers, and has a much simpler structure. It has less concern for the choice of optimum parameters (Breiman 2001; Polikar 2006; Rodriguez-Galiano et al. 2012; Belgiu and Drăguț 2016).

Another concept found in the literature for dealing with big data or high-dimensional feature space is stacked generalization or stacking. Stacking, as an effective decision fusion strategy, involves training a classifier to combine predictions obtained by several other classifiers (Wolpert 1992) (see Figure 1). Waske and Benediktsson (2007) proposed an SVM-based stacking procedure to combine multitemporal SAR and optical imagery. In other studies, SVM-based stacking has also been used for the classification of hyperspectral data (e.g., Chen, Wang, and Wang 2009; Ceamanos et al. 2010). Waske and van der Linden (2008) presented a multilevel object-based SVM procedure for classifying multitemporal SAR and optical data. Employing RF-based, as well as SVM-based, stacking for combining predictions at each level, their results indicated that RF-based stacking was able to offer greater accuracy than the SVM-based version. In all of the above studies, only labels of individual classifiers were used as feature inputs for stacking.

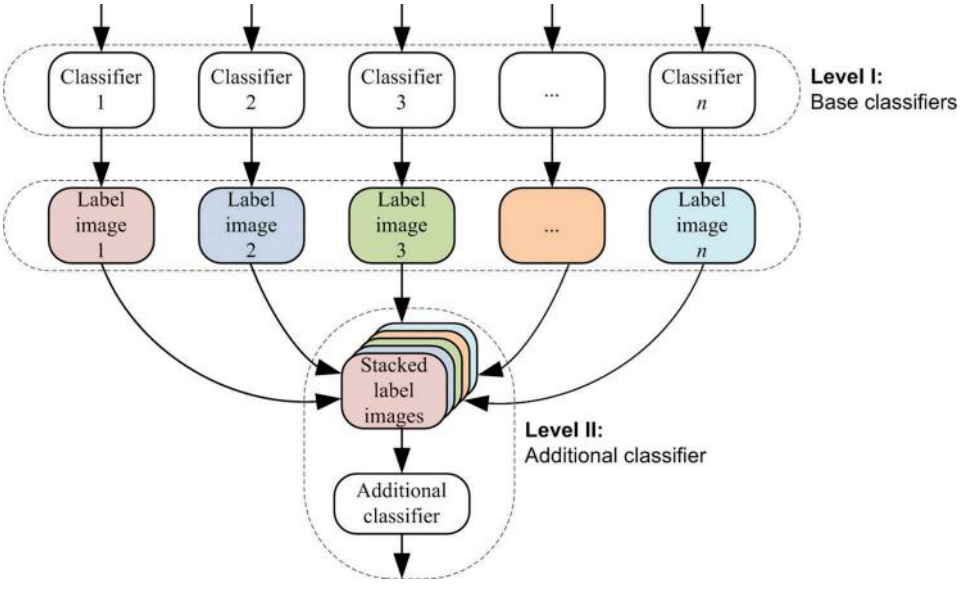

Figure 1. The outline of traditional stacking fusion.

This research work sought to establish an operational framework for crop mapping using bi-temporal of optical and SAR observations. In this context, we examined the capability and effectiveness of a diverse set of spectral, textural and polarimetric features in distinct feature subset groups for the classification of crop lands. The proposed methodology was based on the stacked generalization of an RF classifier. Unlike typical stacking methods, this method employed updated data rather than individual labels as new inputs for stacking. The proposed framework can be very beneficial for the operational crop mapping and monitoring from the freely available optical and radar earth observations, such as Sentinel-1 and -2, Landsat-8 and the future Radarsat Constellation Mission (RCM).

2. Earth observations and study area

The study area of this paper was the southwest district of Winnipeg, Manitoba, Canada, which is covered by various annual crops (see Figure 2). This region is located between from 47° 32′ 16″ to 48° 12′ 56″ N and from 97° 5′ 2″ to 97° 45′ 13″ W. The area of the region is near 400 ha. The mean elevation from sea level is about 784 ft (239 m).

The data used in this paper were bi-temporal optical and radar images acquired by RapidEye satellites and the UAVSAR system. RapidEye is a spaceborne satellite, which has five spectral channels: blue (B), green (G), red (R), NIR and RE. In this paper, two optical images were collected on 5 and 14 July 2012. Both these images were orthorectified on the local North American 1983 datum (NAD-83) with a spatial resolution of about 5 m.

The UAVSAR sensor is an airborne SAR sensor, which operates in the L-band frequency in full polarization mode (i.e., HH, HV, VH and VV). The radar images used in this paper were simultaneously acquired with the optical images. They were orthorectified on the World Geodetic System 1984 datum (WGS-84) with an SRTM3 digital elevation model. They were also multilooked by 2 pixels in azimuth and 3 pixels in range directions. Moreover, the de-speckling process, using a 5×5 boxcar filter, was applied to the data in order to alleviate the speckle effect. The spatial resolution of these images was then approximately 15 m.

The reference data of the study area were collected during the Soil Moisture Active Passive Validation Experiment 2012 (SMAPVEX 2012) campaign for the calibration and validation of National Aeronautics and Space Administration (NASA)'s SMAP satellite (McNairn et al. 2015). The SMAPVEX 12 data collection executed 43 days during the summer of 2012. Indeed, the in situ measurements and earth observations started at the early stages of crop development and finished during the period of maximum biomass accumulation.

According to reference data for the study area, seven classes were found in this region as follows: canola, corn, soybeans, peas, oat, wheat and broadleaf (see Figure 3). The number of samples for each class is presented in Table 1. As can be seen, there is an imbalanced data distribution among the classes. Broadleaf and peas have fewer samples (i.e., minority classes), while other classes have much more samples (i.e., majority classes). In land-cover classification process, the collection of training and test samples is always a challenging and overwhelming task. Therefore, researchers are usually interested in obtaining the high accuracy with the inadequate data. For this purpose, we supposed that the training samples were limited for crop mapping in order to better assess the efficiency and capability of the traditional and proposed methods. In this paper, 5% of all samples, in two scenarios, were randomly stratified selected for the training purpose: (1) when there was a balanced data distribution among the classes and

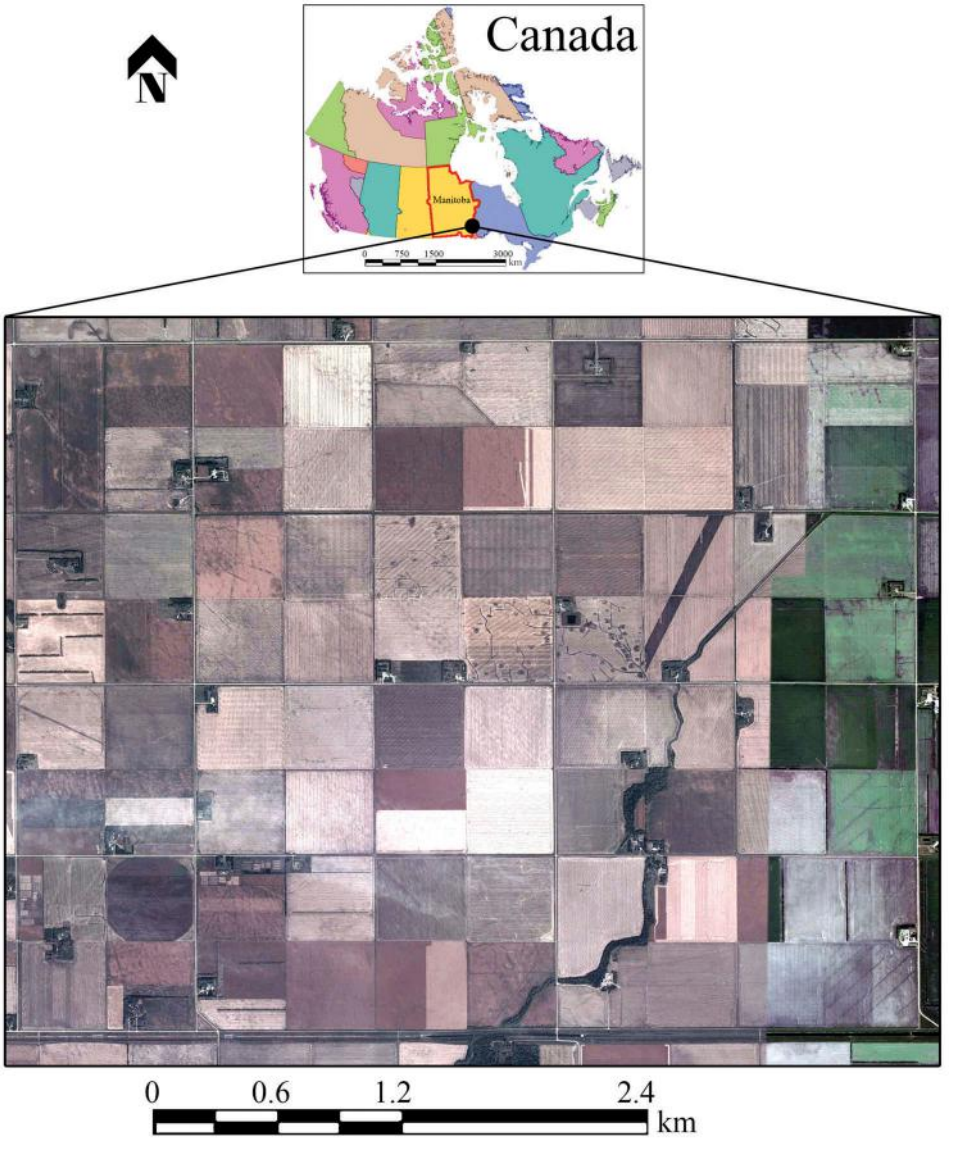

Figure 2. A subset of the study area, Winnipeg, Manitoba, Canada.

(2) when there was an imbalanced data distribution among the classes. These two types of sampling were accomplished in order to investigate the sensitivity of the methods to data distribution. The remaining samples were used for the accuracy assessment.

3. Proposed crop mapping framework

Figure 4 illustrates the proposed crop mapping framework in this paper, based on a decision fusion strategy and the RF classifier from the bi-temporal UAVSAR and RapidEye images. In

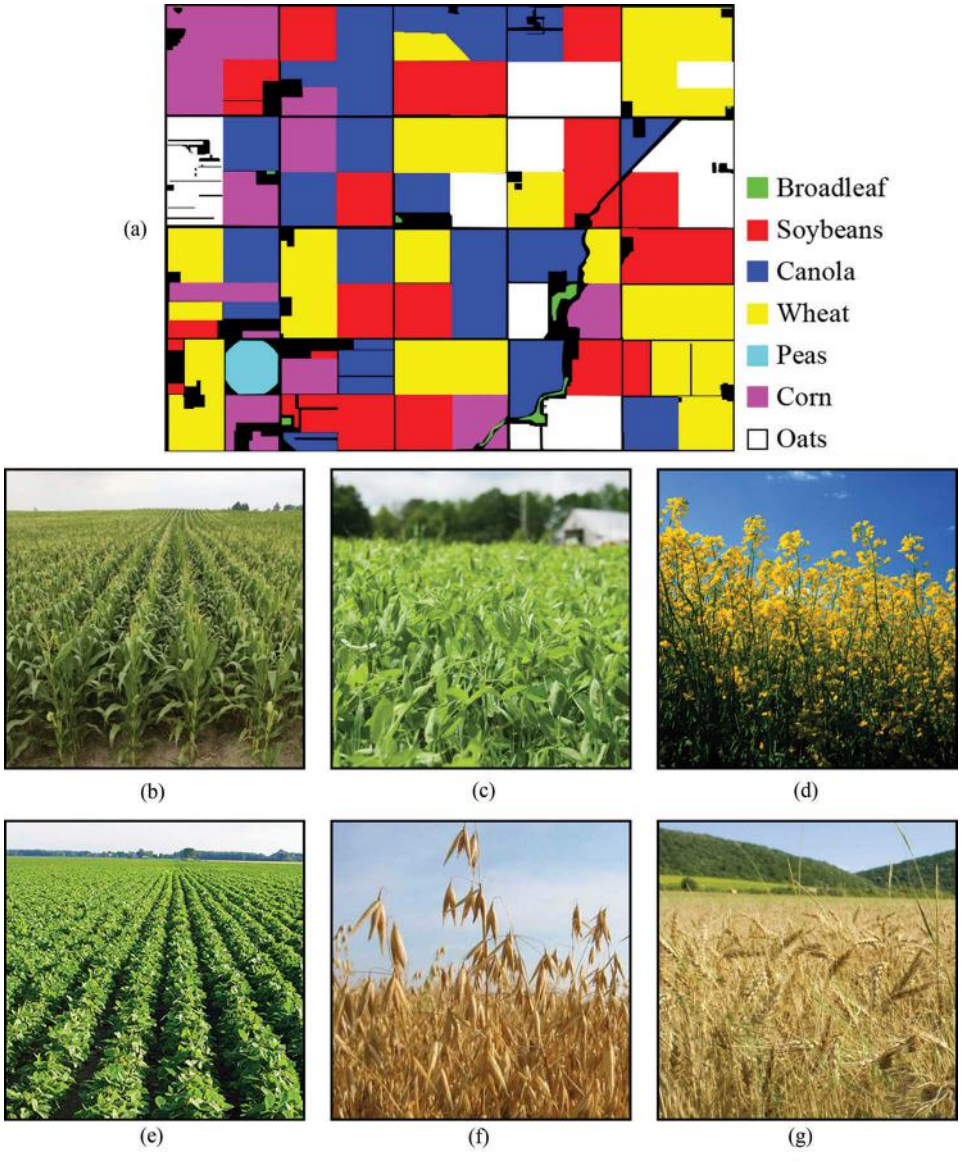

Figure 3. (a) The reference data and (b)–(g) crop types of the experiment region: (b) corn, (c) peas, (d) canola, (e) soybeans, (f) oats, and (g) wheat.

Table 1. The number of all samples (pixels) for the study area.

Class	Corn	Peas	Canola	Soybeans	Oats	Wheat	Broadleaf
No. of samples	39162	3598	75673	74067	47117	85074	1143
No. of balanced training	55	55	55	55	55	55	55
No. of imbalanced training	1960	180	3780	3700	2360	4250	55

the first step, the bi-temporal PolSAR and optical images were efficiently co-registered. The radar images had a coarser resolution; thus, the optical images were warped to be isodiametric with the radar images. Since the radar and optical images were geo-referenced at

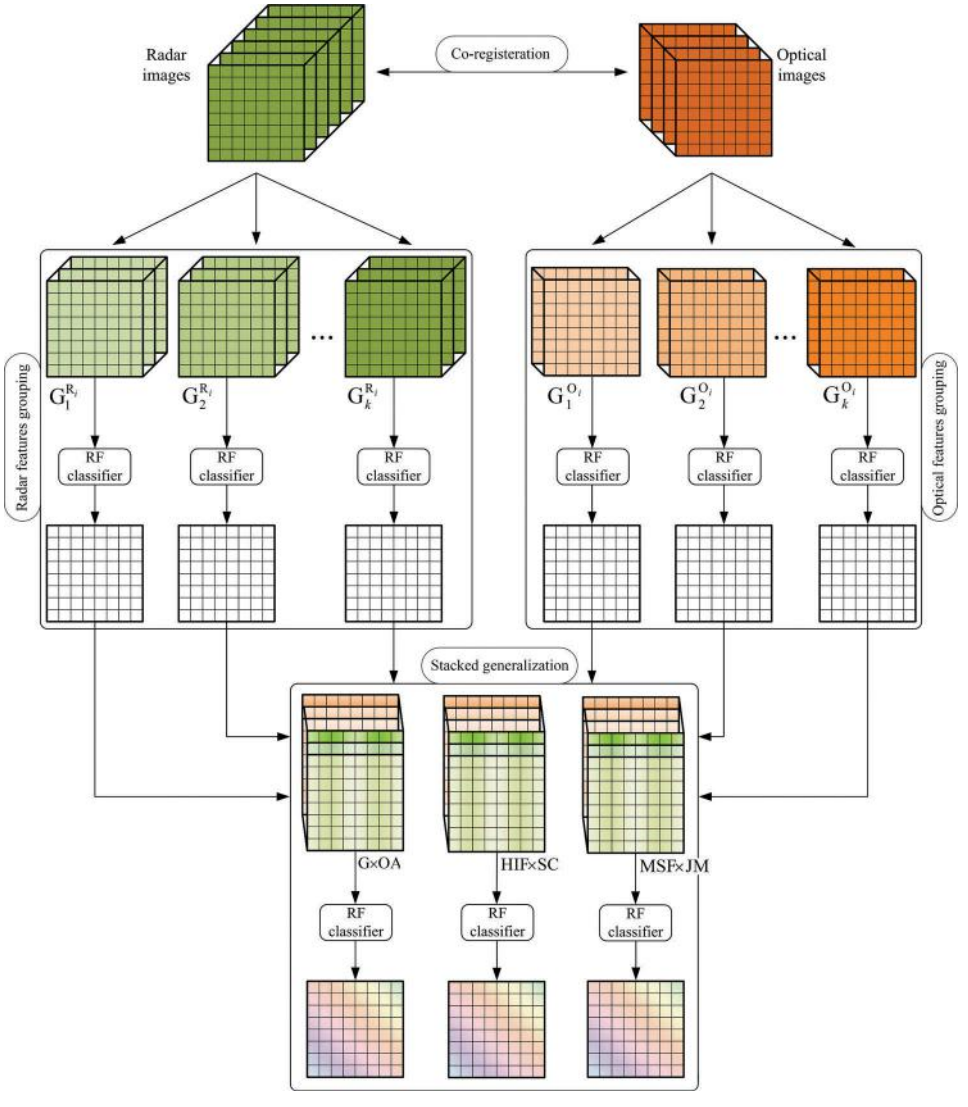

Figure 4. The proposed RF-based framework for crop mapping.

different datums and they had unequal pixel sizes, there were scale, rotation, and translation parameters for co-registering. For this purpose, the polynomial functions with degrees 1 (linear) and 2 (quadratic) were tested and the best results were then chosen based on root mean square error (RMSE). The experiments demonstrated that the quadratic polynomial (with RMSE = 0.36) was better than the linear polynomial (with RMSE = 1.55) for co-registering. In addition, nearest neighbour method was used for grey-level interpolation. Finally, all images had 15m spatial resolution.

Various polarimetric and optical features were then extracted from these images. One of the main goals of this research was to examine the effectiveness of these

features for the classification of croplands in distinct feature subsets. For this purpose, these features were grouped.

Previous studies for band or feature grouping, such as that from Benediktsson and Kanellopoulos (1999), used absolute correlation and a manual clustering to put similar hyper spectral bands together. This strategy was also used by Ceamanos et al. (2010) for dividing a hyperspectral image into several sources. Martinez-Uso et al. (2006) and Guo et al. (2006) used a mutual information measure for the band grouping of multispectral or hyperspectral data. Bigdeli, Samadzadegan, and Reinartz (2013) also used a modified mutual information approach based on a genetic algorithm and an SVM to group the bands of a hyperspectral data set.

In this paper, we manually grouped the features based on their radar and optical natures and definitions. In fact, we put these features into several similar groups (G_i^R or G_j^O). In the next step, each group was classified separately using a unique RF classifier. Finally, three novel stacking fusion strategies, based on an additional RF, were proposed. Unlike traditional stacking methods (Figure 1), updated data were used instead of unique predictions for stacking. In this case, the updated data were built based on overall accuracy values, variable importance scores and Jeffries-Matusita distances.

3.1. Features extraction and grouping

3.1.1. Radar features

A variety of polarimetric features can be extracted from the UAVSAR data, from either the Sinclair scattering matrix (**S**) or the multilooked covariance (**C**) and coherency (**T**) matrices (Tamiminia et al. 2017). In this paper, we extracted the following radar features from the bi-temporal radar images and grouped them into similar groups.

The primary radar features were three linear and three circular polarization intensities ($\boldsymbol{\sigma}_{hh}$, $\boldsymbol{\sigma}_{hv}$ and $\boldsymbol{\sigma}_{vv}$; $\boldsymbol{\sigma}_{rr}$, $\boldsymbol{\sigma}_{rl}$ and $\boldsymbol{\sigma}_{ll}$), which offer information about the structure of various land covers and crop types. They were put into the $G_1^{R_i}$ group (i = {1, 2} indicates the date). In addition, three ratios of linear polarizations ($\boldsymbol{R}_{hhvv}$, $\boldsymbol{R}_{hvhh}$ and $\boldsymbol{R}_{hvvv}$) and three ratios of circular polarizations ($\boldsymbol{R}_{rrll}$, $\boldsymbol{R}_{rlrr}$ and $\boldsymbol{R}_{rlll}$) were extracted and grouped in $G_2^{R_i}$. Six ratios of linear/circular polarizations to total power, i.e., span ($\boldsymbol{R}_{hh}$, $\boldsymbol{R}_{hv}$ and $\boldsymbol{R}_{vv}$; $\boldsymbol{R}_{rr}$, $\boldsymbol{R}_{rl}$ and $\boldsymbol{R}_{ll}$), were also extracted and grouped in $G_3^{R_i}$. These two groups (G_2 and G_3) have proved their capability for land cover and crop mapping (Rignot et al. 1993; Dubois, Van Zyl, and Engman 1995; Entezari, Motagh, and Mansouri 2012).

Other polarimetric parameters, which have proven to be very promising in distinguishing between natural and built-up areas, are correlation coefficients between pairwise polarizations, since their values differ in various land covers (Entezari, Motagh, and Mansouri 2012). Therefore, three linear polarization correlations ($\boldsymbol{\rho}_{hhvv}$, $\boldsymbol{\rho}_{hvhh}$ and $\boldsymbol{\rho}_{hvvv}$) and three circular polarization correlations ($\boldsymbol{\rho}_{rrll}$, $\boldsymbol{\rho}_{rlrr}$ and $\boldsymbol{\rho}_{rlll}$) were extracted from the UAVSAR images and placed into the $G_4^{R_i}$ group.

Other radar features extracted from the UAVSAR data were the statistical feature vectors related to eigenvalues of the **T** matrix input into the $G_5^{R_i}$ group. These features were three eigenvalue decompositions ($\boldsymbol{\lambda}_1$, $\boldsymbol{\lambda}_2$ and $\boldsymbol{\lambda}_3$), as the weight indices of each scattering mechanism. Moreover, some studies have reported a high level of efficiency of their derivatives, including entropy ($\boldsymbol{H}$), anisotropy ($\boldsymbol{A}$) and alpha angle ($\bar{\alpha}$), as well as

four combinations of $\boldsymbol{H}$ and $\boldsymbol{A}$ in discriminating various land covers, especially in natural areas (e.g., Cloude and Pottier 1997; Lee and Pottier 2009; Hoekman, Vissers, and Tran 2011; Entezari, Motagh, and Mansouri 2012; Tamiminia et al. 2017). Two radar vegetation-related feature vectors, i.e., pedestal height ($\boldsymbol{\psi}$) and the radar vegetation index (RVI), are also helpful for vegetation analysis (Samadzadegan and Ferdosi 2012).

In addition to the eigenvalue decompositions, coherent and incoherent target decompositions, which can offer useful information about the physics of scattering mechanisms, were extracted from the UAVSAR imagery.

Coherent decompositions express the scattering matrix as a combination of the scattering responses of simpler targets. We extracted three Pauli parameters ($|\boldsymbol{\alpha}|^2$, $|\boldsymbol{\beta}|^2$ and $|\boldsymbol{\gamma}|^2$) and three Krogager parameters ($|\boldsymbol{k}_s|^2$, $|\boldsymbol{k}_d|^2$ and $|\boldsymbol{k}_h|^2$) as the coherent decompositions, then put them into the $G_6^{R_i}$ group (Cloude and Pottier 1996; Krogager 1990). Incoherent decompositions separate the covariance or coherency matrices into a combination of the second-order descriptors corresponding to simpler or canonical objects. Here, three Freeman-Durden parameters ($\boldsymbol{P}_s$, $\boldsymbol{P}_d$ and $\boldsymbol{P}_v$) and four Yamaguchi parameters ($\boldsymbol{P}_s^{\,Y}$, $\boldsymbol{P}_d^{\,Y}$, $\boldsymbol{P}_v^{\,Y}$ and $\boldsymbol{P}_c^{\,Y}$) were extracted as incoherent decompositions, before being placed in $G_7^{R_i}$ (Freeman and Durden 1998; Yamaguchi et al. 2005). Here, the subscripts 's', 'd', and 'v' denote the surface, double-bounce and volume scattering powers, respectively. Moreover, the subscripts 'h' and 'c' denote the helix scattering power for the Krogager and Yamaguchi (Y) decompositions, respectively. Table 2 provides a list of the radar feature groups mentioned above.

3.1.2. Optical features

From the bi-temporal RapidEye images, three general categories of features (spectral bands, VIs and textural indicators) were extracted and put into several similar groups as follows:

Five spectral bands of RapidEye, i.e., B, G, R, RE and NIR, as the primary optical features, were consolidated in $G_1^{O_i}$. This group has the reflectance information of land covers and crop types in the range of visible to infrared wavelengths. It is worth noting that the RE band, which is a unique to RapidEye satellites, has been designed especially for vegetation characterization (Schuster, Förster, and Kleinschmit 2012).

Moreover, several common VIs were extracted from the RapidEye images. These features are particularly developed for discerning vegetation from other land covers. Here, two VI groups were considered: 1) a set of classical VIs based on R and NIR, including the NDVI, SR, EVI, red-green ratio index (RGRI), atmospherically resistant vegetation index (ARVI), soil adjusted vegetation index (SAVI), normalized difference greenness index (NDGI), green NDVI (gNDVI) and modified triangular vegetation index (MTVI2), were put in $G_2^{O_i}$ (Haboudane et al. 2004; Peña-Barragán et al. 2011; Chellasamy, Zielinski, and Greve 2014; Zhong et al. 2015), 2) a set of VIs based on RE, including the red-edge normalized difference vegetation index (NDVIre), red-edge simple ratio (SRre), red-edge normalized difference greenness index (NDGIre), red-edge triangular vegetation index (RTVIcore), red-edge NDVI (RNDVI), transformed chlorophyll absorption in reflectance index (TCARI), triangular vegetation index (TVI) and red-edge ratio 2 (RRI2), were put in $G_3^{O_i}$ (Löw et al. 2012; Kross et al. 2015).

In addition to the spectral and VI features, textural indicators, which give us information about the relative positions of various grey levels within the image (Haralick and

Table 2. Radar features extracted from the bi-temporal UAVSAR images.

Features and formulas (G: groups, R: radar, i = 1 to 7)	
$G_1^{R_i}$	$\sigma_{hh} = 10\log_{10}\lvert S_{hh}\rvert^2, \sigma_{hv} = 10\log_{10}\lvert S_{hv}\rvert^2, \sigma_{vv} = 10\log_{10}\lvert S_{vv}\rvert^2, \sigma_{rr} = 10\log_{10}\lvert S_{rr}\rvert^2, \sigma_{rl} = 10\log_{10}\lvert S_{rl}\rvert^2, \sigma_{ll} = 10\log_{10}\lvert S_{ll}\rvert^2$ $\{h : \text{horizontal}, v : \text{vertical}, r : \text{right} - \text{handed}, l : \text{left} - \text{handed}\}$
$G_2^{R_i}$	$R_{hhvv} = 10\log_{10}\left(\lvert S_{hh}\rvert^2/\lvert S_{vv}\rvert^2\right), R_{hvhh} = 10\log_{10}\left(\lvert S_{hv}\rvert^2/\lvert S_{hh}\rvert^2\right), R_{hvvv} = 10\log_{10}\left(\lvert S_{hv}\rvert^2/\lvert S_{vv}\rvert^2\right),$ $R_{rrll} = 10\log_{10}\left(\lvert S_{rr}\rvert^2/\lvert S_{ll}\rvert^2\right), R_{rlrr} = 10\log_{10}\left(\lvert S_{rl}\rvert^2/\lvert S_{rr}\rvert^2\right), R_{rlll} = 10\log_{10}\left(\lvert S_{rl}\rvert^2/\lvert S_{ll}\rvert^2\right)$
$G_3^{R_i}$	$R_{hh} = 10\log_{10}\left(\lvert S_{hh}\rvert^2/\text{span}\right), R_{hv} = 10\log_{10}\left(\lvert S_{hv}\rvert^2/\text{span}\right), R_{vv} = 10\log_{10}\left(\lvert S_{vv}\rvert^2/\text{span}\right),$ $R_{rr} = 10\log_{10}\left(\lvert S_{rr}\rvert^2/\text{span}\right), R_{rl} = 10\log_{10}\left(\lvert S_{rl}\rvert^2/\text{span}\right), R_{ll} = 10\log_{10}\left(\lvert S_{ll}\rvert^2/\text{span}\right)$ $\left\{\text{span} = \lvert S_{hh}\rvert^2 + 2\lvert S_{hv}\rvert^2 + \lvert S_{vv}\rvert^2 = \lvert S_{rr}\rvert^2 + 2\lvert S_{rl}\rvert^2 + \lvert S_{ll}\rvert^2\right\}$
$G_4^{R_i}$	$\rho_{hhvv} = \left\lvert \frac{S_{hh}.S_{vv}^*}{\sqrt{\left(S_{hh}.S_{hh}^*\right)\left(S_{vv}.S_{vv}^*\right)}} \right\rvert, \rho_{hvhh} = \left\lvert \frac{S_{hv}.S_{hh}^*}{\sqrt{\left(S_{hv}.S_{hv}^*\right)\left(S_{hh}.S_{hh}^*\right)}} \right\rvert, \rho_{hvvv} = \left\lvert \frac{S_{hv}.S_{vv}^*}{\sqrt{\left(S_{hv}.S_{hv}^*\right)\left(S_{vv}.S_{vv}^*\right)}} \right\rvert,$ $\rho_{rrll} = \left\lvert \frac{S_{rr}.S_{ll}^*}{\sqrt{\left(S_{rr}.S_{rr}^*\right)\left(S_{ll}.S_{ll}^*\right)}} \right\rvert, \rho_{rlrr} = \left\lvert \frac{S_{rl}.S_{rr}^*}{\sqrt{\left(S_{rl}.S_{rl}^*\right)\left(S_{rr}.S_{rr}^*\right)}} \right\rvert, \rho_{rlll} = \left\lvert \frac{S_{rl}.S_{ll}^*}{\sqrt{\left(S_{rl}.S_{rl}^*\right)\left(S_{ll}.S_{ll}^*\right)}} \right\rvert$ $\{* : \text{complex conjugate}, . : \text{vector dot product}\}$
$G_5^{R_i}$	$\lambda_1, \lambda_2, \lambda_3, \quad H = -\sum_{i=1}^{3} p_i \log_3 p_i, A = (\lambda_2 - \lambda_3)/(\lambda_2 + \lambda_3), \bar{\alpha} = \sum_{i=1}^{3} p_i a_i \quad \left\{p_i = \lambda_i \Big/ \sum_{k=1}^{3} \lambda_k\right\}$ $HA, H(1-A), (1-H)A, (1-H)(1-A), \quad \psi = \min(\lambda_1, \lambda_2, \lambda_3)/(\lambda_1 + \lambda_2 + \lambda_3), \text{RVI} = 4\lambda_3/(\lambda_1 + \lambda_2 + \lambda_3)$
$G_6^{R_i}$	$\lvert\alpha\rvert^2 = \frac{\sqrt{2}}{2}\lvert S_{hh} + S_{vv}\rvert^2, \lvert\beta\rvert^2 = \frac{\sqrt{2}}{2}\lvert S_{hh} - S_{vv}\rvert^2, \lvert\gamma\rvert^2 = 2\lvert S_{hv}\rvert^2, \lvert k_s\rvert^2 = \lvert S_{rl}\rvert^2, \lvert k_d\rvert^2 = \min\left(\lvert S_{rr}\rvert^2, \lvert S_{ll}\rvert^2\right), \lvert k_h\rvert^2 = \text{abs}\left(\lvert S_{rr}\rvert^2 - \lvert S_{ll}\rvert^2\right)$ $\{s : \text{surface scattering}, d : \text{double} - \text{bounce scattering}, h : \text{helix scattering}\}$
$G_7^{R_i}$	$P_s = f_s(1 + \lvert\beta\rvert^2), P_d = f_d(1 + \lvert\alpha\rvert^2), P_v = f_v, P_s^Y = f_s(1 + \lvert\beta\rvert^2), P_d^Y = f_d(1 + \lvert\alpha\rvert^2), P_v^Y = f_v, P_c^Y = f_c$ $\{v : \text{volume scattering}, c : \text{helix scattering}\}$

Shanmugam 1973), were extracted from the RapidEye images. In this paper, eight main parameters of the grey-level concurrence matrix (GLCM), i.e., mean ($\boldsymbol{\mu}$), variance ($\boldsymbol{\sigma}$), homogeneity (HOM), contrast (CON), dissimilarity (DIS), entropy ($\boldsymbol{H}$), angular second moment (ASM) and correlation (COR), were used to describe the textural information (Theodoridis and Koutroumbas 2003). Kim and Yeom (2014) have shown that the GLCM of RE and NIR bands can be useful in improving crop mapping accuracy. However, in this case, we initially employed a principle component analysis (PCA) to the spectral bands and then chose the principal components (PCs) with the highest information content. We used PC1 and PC2 for both RapidEye images, since they contained 99.03% and 98.35% of all information in all the bands, respectively. Then, the GLCM was applied to these two features, rather than all the spectral bands, in order to reduce the dimensionality of data. Moreover, our experiment indicated that these textural features were able to produce higher accuracy than the textural features obtained by the RE and NIR bands. Finally, we put the PC1-based GLCM in$G_4^{O_i}$ and the PC2-based GLCM in$G_5^{O_i}$. The five above-mentioned optical groups are presented in Table 3.

3.2. Random forest algorithm

For classifying each of the radar and optical groups, we used a standard RF classifier. Developed by Breiman (2001), the RF algorithm is an ensemble of decision trees. In fact, an RF combines a multitude of diverse decision trees to reduce the risk of overfitting. The RF trains these decision trees in parallel separately. This algorithm injects randomness into two steps of the training process. Firstly, training samples are divided into

Table 3. Optical features extracted from the bi-temporal RapidEye images.

Features and formulas (G: groups, O: optical, i = 1 to 5)	
$G_1^{O_i}$	R_B: 440 − 510nm, R_G: 520 − 590nm, R_R: 630 − 685nm, R_{RE}: 690 − 730nm, R_{NIR}: 760 − 850nm R: Reflectance
$G_2^{O_i}$	$NDVI = (R_{NIR} - R_R)/(R_{NIR} + R_R)$
	$SR = R_{NIR}/R_R$
	$RGRI = R_G/R_R$
	$EVI = 2.5(R_{NIR} - R_R)/(R_{NIR} + 6R_R - 7.5R_B + 1)$
	$ARVI = (R_{NIR} - (2R_R - R_B))/(R_{NIR} + (2R_R - R_B))$
	$SAVI = (1 + 0.5)(R_{NIR} - R_R)/(R_{NIR} + R_R + 0.5)$
	$NDGI = (R_G - R_R)/(R_G + R_R)$
	$gNDVI = (R_{NIR} - R_G)/(R_{NIR} + R_G)$
	$MTVI2 = 1.5(1.2(R_{NIR} - R_G) - 2.5(R_R - R_G))/\sqrt{(2R_{NIR} + 1)^2 - (6R_{NIR} - 5\sqrt{R_R}) - 0.5}$
$G_3^{O_i}$	$NDVIre = (R_{NIR} - R_{RE})/(R_{NIR} + R_{RE})$
	$SRre = R_{NIR}/R_{RE}$
	$NDGIre = (R_G - R_{RE})/(R_G + R_{RE})$
	$RTVIcore = 100(R_{NIR} - R_{RE}) - 10(R_{NIR} - R_G)$
	$RNDVI = (R_{RE} - R_R)/(R_{RE} + R_R)$
	$TCARI = 3((R_{RE} - R_R) - 0.2(R_{RE} - R_G)(R_{RE}/R_R))$
	$TVI = 0.5(120(R_{RE} - R_G) - 200(R_R - R_G))$
	$PRI2 = R_{RE}/R_R$
$G_4^{O_i}$	$\mu_{PC1}, \sigma_{PC1}, HOM_{PC1}, CON_{PC1}, DIS_{PC1}, H_{PC1}, ASM_{PC1}, COR_{PC1}$ from GLCM of PC1
$G_5^{O_i}$	$\mu_{PC2}, \sigma_{PC2}, HOM_{PC2}, CON_{PC2}, DIS_{PC2}, H_{PC2}, ASM_{PC2}, COR_{PC2}$ from GLCM of PC2

several subsamples (nTrees) by a random sampling method, i.e., a bootstrapping method. A subset of features (mTry) from all features for each subsample is then chosen by a random subset feature selection method (Breiman 2001). In this paper, 500 was considered for nTrees. The root square of the number of features in each radar or optical group, as mentioned in the previous section, was considered for mTry, according to Breiman (2001).

In the prediction process for a test sample, the RF combines the outputs or labels of individual decision trees using a classical majority voting technique. This voting technique chooses class w_k for sample p, when this class receives the highest number of votes among all votes obtained by all decision trees (Khosravi et al. 2017). Mathematically, class w_k is chosen by the majority voting technique, if:

$$\sum_{i=1}^{L} d_{i,k} = \max_{j=1}^{c} \sum_{i=1}^{L} d_{i,j} \tag{1}$$

where $d_{i,j} \in \{0, 1\}$ is the decision value of the i^{th} decision tree for class w_j $\{i = 1, 2, 3, \ldots, L; j = 1, 2, 3, \ldots, c\}$, and L and c are the number of decision trees and classes, respectively. Here, $d_{i,j} = 1$, if the i^{th} decision tree chooses class w_j, and 0 otherwise.

The RF algorithm does have a particular capability, the so-called 'variable importance', which is the ranking of features in a classification task. For determining the importance of a given feature, at first, the out-of-bag error (OOBE) is computed during the training process. The OOBE is the mean prediction error on each training sample x_i, using only the decision trees that have been trained by the bootstrap sample in which x_i is absent. After training, the values of that feature are then permuted among the training data, and the OOBE is re-computed using these perturbed data. The importance score for this feature is thus determined by averaging the difference of the OOBE before and after the permutation over all decision trees. The score can be normalized by the standard deviation of these differences (James et al. 2013).

3.3. Decision fusion strategies: stacking algorithm

Stacking decision fusion consists of training a classifier in order to combine the predictions of several other classifiers. First, all other algorithms are trained using the available data. Then, all the predictions of these algorithms, as new inputs, are used for an additional classification using a combiner algorithm to make a final prediction (Wolpert 1992).

In this paper, we proposed three stacking strategies to fuse the results of individual RF classifiers. The combiner in this case was an additional RF classifier. Unlike traditional stacking algorithms, we did not use the outputs of individual RFs as the inputs of the additional RF. Instead, we used an updated data for each strategy (see Figure 3). The proposed strategies were as follows:

3.3.1. Strategy 1 (group × overall accuracy)

In Strategy 1, after the classification of each radar and optical features group, the data were updated as follows: each group (G_k) was firstly multiplied by the overall accuracy (OA_k) obtained by the trained RF using that group. All the weighted groups were then stacked together (G × OA). Finally, these updated data were reclassified by an additional RF

algorithm. This process can be justified as follows: each features group that has obtained higher OA has to be assigned a higher weight in the additional classification task.

3.3.2. Strategy 2 (highest important features × importance score)

In this strategy, the data were updated as follows: in parallel to the classification of each group, the mTry number of highest important features (HIF_k) was chosen, based on the variable importance property. Then, these highest important features of each group were multiplied by their related importance scores (SC_k) and stacked together (HIF × SC). Finally, the updated data were reclassified by an additional RF algorithm.

3.3.3. Strategy 3 (most separable features × separation value)

In Strategy 3, the data were updated as follows: before the classification of each group, the mTry number of the most separable features (MSF_k) was chosen using an efficient separation measure. In this paper, the Jeffries-Matusita (JM) distance, as an efficient and common measure of separation in the classification task, was employed. This distance can determine the separability of two classes for a given feature as follows (Zhang et al. 2016):

$$JM = 2(1 - \exp(-B)) \tag{2}$$

where B is the Bhattacharyya distance value defined as follows (Zhang et al. 2016):

$$B = \frac{1}{8}(\mu_1 - \mu_2)^2 \frac{2}{\sigma_1^2 + \sigma_2^2} + \frac{1}{2}\ln\left(\frac{\sigma_1^2 + \sigma_2^2}{2\sigma_1\sigma_2}\right) \tag{3}$$

where μ_i and σ_i (i = 1,2) are the mean and variance for two classes and a feature. The JM-value is in the range of [0, 2]. Zero indicates the weakest separation, while 2 indicates the highest separation among the classes for that feature (Zhang et al. 2016). After computing the JM-values, the most separable features of each group were multiplied by their mean JM-values over classes (JM_i) and then stacked together (MSF × JM). The updated data were finally reclassified by an additional RF algorithm.

4. Implementation and results

In this section, the individual RF algorithms using radar groups, optical groups, and the combination of radar and optical groups were implemented on the data. Then, the traditional and the proposed stacking methods were also implemented. To assess accuracy, this paper employed OA, the kappa coefficient (κ) and F-score metrics extracted from the confusion matrix. OA is a general metric for the evaluation of any classification algorithms. It is the ratio of the correct pixels (the diagonal elements of the confusion matrix) to all samples. This metric cannot well express the reliability and efficiency of the classification algorithms by itself. The $\kappa\kappa$is computed to determine whether the values in a confusion matrix are significantly better than the values in a random assignment. F-score is the harmonic mean of the producer's and user's accuracies in each class and can offer a realistic assessment of the classification task, compared to OA and κ (Congalton 1991; Powers 2011). A recent study reported that acceptable and standard accuracy for crop mapping is F-score ≥85% for all crops (Zhou et al. 2017). Table 4 to 11 present the OA, κ and F-score values of all the individual RFs

Table 4. The OA and κ of the individual RFs using radar features.

	Balanced		Imbalanced			Balanced		Imbalanced	
	OA(%)	κ	OA(%)	κ		OA(%)	κ	OA(%)	κ
$G_1^{R_1}$	57.73	0.54	63.38	0.60	$G_1^{R_2}$	74.75	0.71	79.87	0.77
$G_2^{R_1}$	51.82	0.48	57.02	0.53	$G_2^{R_2}$	52.00	0.48	51.84	0.48
$G_3^{R_1}$	48.91	0.46	56.92	0.53	$G_3^{R_2}$	51.72	0.48	49.40	0.46
$G_4^{R_1}$	51.40	0.48	54.68	0.51	$G_4^{R_2}$	42.31	0.39	49.17	0.45
$G_5^{R_1}$	55.40	0.52	57.26	0.54	$G_5^{R_2}$	77.12	0.74	78.14	0.75
$G_6^{R_1}$	50.18	0.46	55.86	0.52	$G_6^{R_2}$	57.33	0.53	62.13	0.58
$G_7^{R_1}$	52.48	0.49	56.30	0.53	$G_7^{R_2}$	65.00	0.61	69.49	0.66
R_1	65.10	0.61	66.55	0.63	R_2	81.57	0.78	78.88	0.76
$R = [R_1, R_2]$	86.52	0.84	87.67	0.85					

and the proposed stacking methods. Figures 5 and 6 also demonstrate the classification maps of the methods.

Furthermore, in order to evaluate the significance of a difference between the traditional and the proposed stacking results, McNemar's test was utilized. This statistical test was calculated as $z = (\boldsymbol{c}_{12} - \boldsymbol{c}_{21}) \times (\boldsymbol{c}_{12} + \boldsymbol{c}_{21})^{-0.5}$, where $\boldsymbol{c}_{12}$ are the pixels that are correctly classified in the proposed result, but misclassified in the traditional result and vice versa for $\boldsymbol{c}_{21}$. If $|z| \geq 1.96$, the difference is then significant (Braun, Weidner, and Hinz 2012). Table 12 presents the results of this test.

5. Discussion

5.1. Radar feature groups

From Table 4, one can see that the radar groups obtained less than 64% and 0.6 for the OA and the κ, on date 1, respectively. Among these groups, the G_1 group (intensity features) had the highest OA and κ, either with the balanced or with the imbalanced training samples. However, G_3 (ratio features) and G_4 (correlation features) groups had the lowest OA and κ with the balanced and imbalanced training samples, respectively. On date 2, the OA and κ of all radar groups, except for the G_4 group, increased to 80% and 0.8, respectively. The highest OA and κ values belonged to G_5 (eigenvalue-related features) with the balanced training samples, and to G_1 (intensities features) with the imbalanced ones. These results were in line with previous studies reporting the high capability of polarization intensities and eigenvalue-related features (especially H/A/$\bar{\alpha}$). Again, the G_4 group (correlation group) obtained the lowest OA and κ with both the training samples. Table 8 also shows the lower accuracy values (F-score <20%) for the broadleaf class in three groups of G_2, G_3 and G_4. Generally speaking, the correlation coefficients and ratio features had the lowest efficiency and performance among the radar features for crop mapping in our study area.

Regarding the performance of the target decompositions groups, we observed that the OA and κ values of G_7, i.e., incoherent decompositions were higher than those of G_6 i.e., coherent decompositions on both dates with the imbalanced training samples. Therefore, the incoherent decompositions seem to be better than the coherent decompositions for crop mapping in our study area. This conclusion has also been confirmed by the previous studies addressing the advantages of incoherent decompositions for classifying natural

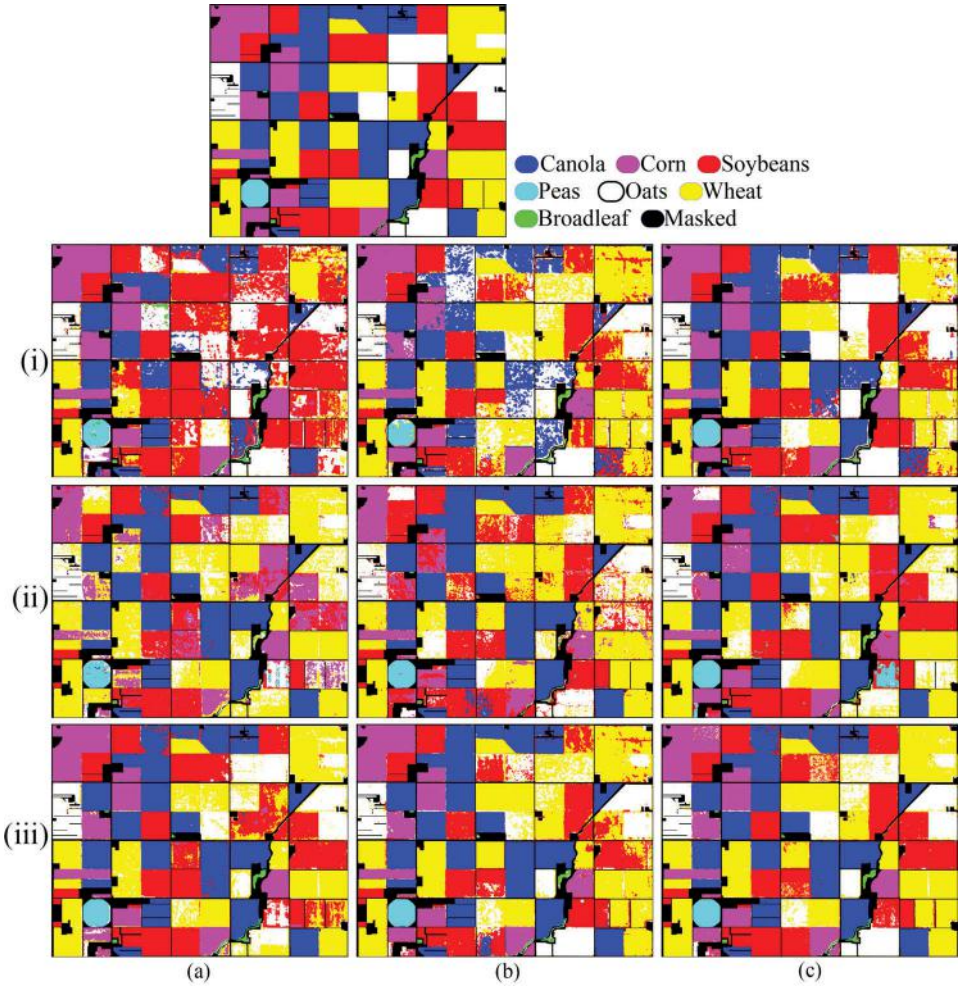

Figure 5. The classification maps obtained from (i) the stacked radar features, (ii) the stacked optical features, and (iii) the combination of radar and optical features using RF with the imbalanced training samples at: (a) date 1, (b) date 2, and (c) the combination of both dates.

targets (e.g., Alberga, Satalino, and Staykova 2008; McNairn et al. 2009a; Tamiminia et al. 2017). It is noteworthy that none of the radar groups was able to achieve standard accuracy, i.e., *F*-score ≥85% for all the crop types in the study area (see Table 8).

Table 4 reported that the accuracy was improved when the radar groups were stacked. For example, the OA of the stacked radar groups reached up to 67% and 82% for dates 1 and 2, respectively. It can thus be concluded that the stacked radar features of date 2 (R_2) have higher levels of performance and efficiency compared to date 1 (R_1) for crop mapping in our study. Moreover, when the stacked radar features of both dates were combined ($R = [R_1, R_2]$), the OA increased to 87% and 88% with the balanced and imbalanced training samples, respectively. This combination led to improvements in the detection rate of all the classes, especially broadleaf, oat and wheat, which had a much lower accuracy in most of the

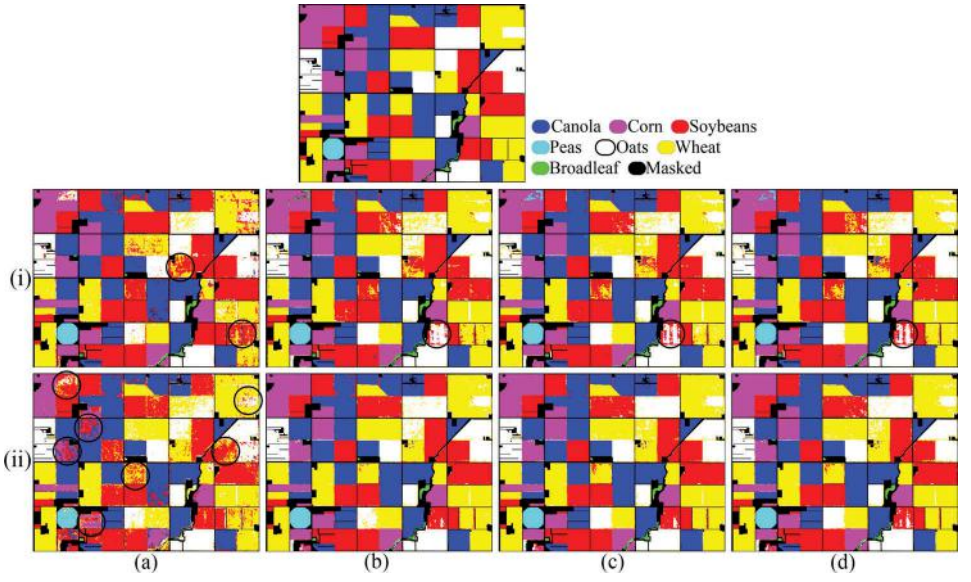

Figure 6. The classification maps obtained by: (a) the traditional, and (b)–(d) the proposed stacking methods with (i) the balanced, and (ii) the imbalanced training samples.

individual groups. Nevertheless, the standard accuracy has not been achieved for all the crops as yet, either with the balanced or with the imbalanced training samples (see Table 8).

Figure 5(a)(i) demonstrated that, with the imbalanced training samples, the R_1 map mixed some oat pixels with canola and soybeans. Furthermore, there were a few mixed pixels of oat and wheat. In the R_2 map, a larger number of oat pixels were mixed with wheat and canola. Meanwhile, wheat and soybeans were again mixed up together on both dates. However, the R map had fewer isolated misclassified pixels than each date and was more uniform.

5.2. Optical feature groups

The OA and the κ under 80% and 0.8 are reported in Table 5 for the optical feature groups. In contrast to the radar groups, the accuracy values of all the optical groups, except for G_1 (spectral bands) in the first date, were higher than those in the second date. However, similar to the radar groups, none of the optical groups could achieve standard accuracy for all the crop types in the study area (see Table 9).

In detail, the maximum OA and κ values belonged to G_3 (VIs based on RE) and G_1 (spectral bands) for the first and second dates, respectively, either with the balanced or with the imbalanced training samples. These results confirmed the role of RE band in the spectral bands of RapidEye and vegetation indices for crop mapping in the study area.

The lowest accuracy on both dates belonged to G_5 (GLCM of PC2) with a κ in the range of [0.3, 0.4]. We can thus conclude that the textural indicators are not suitable features by themselves for crop mapping in our study area.

Regarding VI performance, the VIs-RE group (G_3) was more successful than the classical VIs group (G_2) on both dates. The OA values of this group were 10–15% higher. Meanwhile,

Table 5. The OA and κ of the individual RFs using optical features.

	Balanced		Imbalanced			Balanced		Imbalanced	
	OA(%)	κ	OA(%)	κ		OA(%)	κ	OA(%)	κ
$G_1^{O_1}$	67.25	0.63	71.63	0.67	$G_1^{O_2}$	74.10	0.71	79.67	0.76
$G_2^{O_1}$	64.16	0.60	68.70	0.64	$G_2^{O_2}$	42.96	0.39	55.91	0.51
$G_3^{O_1}$	73.24	0.69	74.66	0.71	$G_3^{O_2}$	55.01	0.52	71.14	0.67
$G_4^{O_1}$	49.12	0.45	60.36	0.55	$G_4^{O_2}$	45.98	0.42	51.64	0.47
$G_5^{O_1}$	41.43	0.37	47.51	0.42	$G_5^{O_2}$	38.14	0.34	45.53	0.41
O_1	71.11	0.67	72.53	0.68	O_2	75.28	0.72	80.23	0.77
$O = [O_1, O_2]$	82.75	0.80	86.02	0.83					

the VIs-RE group was able to detect 30% more corn and peas than its competitor. Thus, we may prefer the VIs-RE to the classical VIs for distinguishing wheat from oat.

Another conclusion could be drawn from the Tables 4 and 5, the stacked optical groups of date 1 (O_1) obtained higher OA and κ values than the stacked radar groups of first date (R_1) either with the balanced or with the imbalanced training samples. Regarding the second date, the stacked radar groups (R_2) had higher accuracy than the stacked optical groups (O_2) with the balanced training samples, and vice versa with the imbalanced training samples. By contrast, the stacked radar features of both dates (R) could obtain higher OA and κ values than the stacked optical groups of both dates (i.e., $O = [O_1, O_2]$) either with the balanced or with the imbalanced training samples. Like radar, none of the O_1, O_2 and O features could obtain standard accuracy for all the crop types in the study area.

In Figure 5(a)(ii), with the imbalanced training samples; unlike the R_1 features, the O_1 features mixed some pixels of corn and soybeans, and wheat and oat. Also, a few corn pixels were also mixed up with wheat. On date 2, in addition to the mixing of wheat and oat pixels, a few soybean pixels were mixed with either wheat or oat. The mixture of wheat and oat can be relatively normal in the optical images because these two crop types have very similar reflectance behaviours, especially on these dates, i.e. summer (Roosjen et al. 2016). For distinguishing wheat from oat, the radar features are thus more suitable than the optical features. The O map had a more homogeneous appearance than each of the O_1 and O_2 maps, while the problems mentioned above, especially the mixing of wheat and oat, were more efficiently eliminated. Nonetheless, a large number of soybean pixels (equivalent to a farm) were wrongly classified as corn.

Another result concerned the mixing of broadleaf (as a minority class) and other classes (especially majority classes); this problem was much less significant in the maps of the optical features than in those of the radar features. Therefore, the optical features were more qualified than the radar features for distinguishing broadleaf from other classes. Furthermore, the maps of all the optical groups had more homogeneous and favourable appearances than the maps of all the radar groups, even though the OA values of O_1 and O features were slightly less than those of their radar competitors. One can see that there were fewer isolated misclassified pixels on the maps of the optical features. This issue is justifiable because of the speckle noise in radar images and the lack of such noise in optical images.

5.3. Combination of optical and radar groups

The combination of all the radar and optical features could increase the OA and the κ values of classification, compared to each of them (see Table 6). In the combination of

Table 6. The OA and κ of the individual RFs using combination of optical and radar features.

	Balanced		Imbalanced	
	OA(%)	κ	OA(%)	κ
R_1O_1 = [R_1, O_1]	85.00	0.82	88.61	0.86
R_2O_2 = [R_2, O_2]	85.11	0.82	87.94	0.86
RO = [R, O]	88.10	0.86	91.52	0.90

the radar and optical features on date 1 (R_1O_1), the OA was 20% higher than for the R_1 features and 15% higher than for the O_1 features (with both the balanced and imbalanced samples). On date 2 (R_2O_2), the OA was 3% and 9% higher than that for the R_2 features and 10% and 8% (with the balanced and imbalanced training samples, respectively) higher than that for the O_2 features. Furthermore, the combination of bi-temporal radar and optical features (RO) increased the OA and κ values to 88% and 0.86 (balanced way), and up to 92% and 0.90 (imbalanced way).

Figure 5(a)(iii)–(b)(iii) indicated that the classification maps of the combination of the radar and optical features with the imbalanced training samples were more favourable and homogeneous, compared to each of them. This advantage was more comprehensible when compared to the results of the radar features. In fact, the well-known salt-and-pepper effect in these maps was much less observable than in the maps of the radar features. For example, with the imbalanced training samples, the corn, canola, peas and broadleaf were detected more perfectly and homogeneously by the R_2O_2 features than the R_2 and O_2 features. The confusion of canola and peas no longer existed, compared to the R_2 map. In addition, the mixed pixels of wheat and soybeans and of wheat and oat were much fewer than on the O_2 map.

Until now, we have only obtained the best classification results with the combination of bi-temporal radar and optical features (see Figure 5(c)(iii)). Most of crop types were detected more homogeneously. The final maps were also less affected by the salt-and-pepper effect. In spite of these advantages, standard accuracy has not been achieved for all the crop types as yet. The *F*-score values of wheat and oat classes were still less than 85% (see Table 10). Meanwhile, there were still some mixed pixels of wheat and soybeans or wheat and oat on the final maps with the imbalanced training samples.

5.4. Stacking methods

As can be seen in Table 7, the OA and κ values of the three proposed stacking methods were higher than all the radar and optical groups. They were also higher than he stacked radar features or the stacked optical features or their combinations. Compared to the RO features, the OA was 2% and 4% higher with the balanced and imbalanced training samples, respectively. In addition, the differences in accuracy values between the proposed and the traditional stacking methods were more striking (e.g., 5% and 12% in OA). McNemar's test indicated a $|z|$ value greater than 1.96 for all three proposed methods versus the traditional method (see Table 12). This issue implies that these differences are significant and meaningful.

It's noteworthy that the traditional stacking method obtained a greater accuracy with the balanced training samples rather than imbalanced ones, unlike most of the other

Table 7. The OA and κ of the traditional and the proposed stacking methods.

	Balanced		Imbalanced	
	OA(%)	κ	OA(%)	κ
Traditional Stacking	85.07	0.82	83.84	0.81
Strategy 1: G × OA	90.33	0.88	95.40	0.94
Strategy 2: HIF × SC	90.42	0.88	94.23	0.93
Strategy 3: MSF × J	90.15	0.88	94.16	0.93

methods. In addition, the traditional stacking method was less accurate than the combination of radar and optical features, implying the incapability of the traditional method. Consequently, the traditional method could not achieve standard accuracy for all crop types. Instead, we were finally able to obtain an acceptable level of accuracy (higher than 85%) for all the crop types, only by the proposed methods with the 5% imbalanced training samples.

In terms of *F*-score, the values of the proposed methods were relatively higher than those of the traditional method. Of course with the balanced training samples, the *F*-score of broadleaf obtained by the traditional method was 9% and 16% greater than by the proposed methods. By contrast, with the imbalanced ones, its value was about 56% lower than the proposed methods (see Table 11).

Figure 6 also confirmed the higher visual advantage of the classification maps obtained by the proposed methods compared to the other methods especially traditional method, either with the balanced or with the imbalanced training samples.

With the balanced training samples, there were a large number of mixed pixels, especially wheat and soybeans, and wheat and oat. Even, two wheat farms were wrongly classified as soybeans farms (see back circles at Figure 6(a)(i)). By contrast, most of these mixed pixels were efficiently omitted in the classification maps of the proposed methods. In addition, those wrong classified farms were correctly as wheat in the proposed maps. However, a small soybeans farm was wrongly detected as oats in the proposed maps especially in the strategy 1's map (see back circles at Figure 6(b)(i), (c)(i), and (d)(i)).

With the imbalanced training samples, the map obtained by the traditional method was more unfavourable than before. Although those soybeans misclassified farms were correctly classified in this map, an abundant number of soybeans and corn, soybeans and canola, soybeans and wheat, and wheat and oats pixels were mixed together. They are shown in Figure 6(a)(ii) by black circles. By contrast, most of these mixed pixels, especially wheat and oats, and wheat and soybeans, were correctly classified in the proposed maps. These maps were more continuous in spatial terms and more homogeneous. They were also almost unaffected by the salt-and-pepper effect (see Figure 6(b)(ii), (c)(ii), and (d)(ii)).

The performance and the results of the three proposed stacking methods were comparatively similar. However, with the balanced training samples, the second strategy (the use of the highest importance features of each group) and, with the imbalanced samples, the first strategy (the use of the OA of each group) had the best efficiency and results among all the proposed strategies.

Table 8. The *F*-score of the individual RFs using radar features.

	Balanced							Imbalanced						
	Corn	Peas	Canola	Soybeans	Oats	Wheat	Broadleaf	Corn	Peas	Canola	Soybeans	Oats	Wheat	Broadleaf
$G_1^{R_1}$	71.95	83.57	75.60	58.88	41.15	37.24	21.18	83.53	84.59	76.36	64.86	52.08	41.74	50.39
$G_2^{R_1}$	61.29	72.20	40.92	64.86	46.83	43.53	6.95	59.96	82.21	50.64	64.67	53.94	51.41	9.51
$G_3^{R_1}$	52.86	70.81	42.48	59.65	46.91	41.35	6.74	57.24	80.41	49.82	65.21	54.85	51.88	7.16
$G_4^{R_1}$	74.18	78.64	40.25	64.53	40.02	39.98	6.16	75.49	78.41	42.56	68.77	40.62	45.98	20.44
$G_5^{R_1}$	85.24	85.37	57.33	53.00	58.12	35.72	20.43	87.05	87.55	62.20	55.96	50.51	39.89	69.80
$G_6^{R_1}$	64.53	81.23	64.35	50.03	35.97	35.23	24.97	69.90	82.78	66.05	57.76	46.54	39.79	40.53
$G_7^{R_1}$	65.21	90.16	63.99	49.21	52.64	34.33	34.13	68.28	91.07	64.03	51.02	58.11	44.27	55.47
$G_1^{R_2}$	91.15	88.60	85.90	70.86	59.89	69.83	45.03	94.52	91.12	91.83	76.82	62.67	75.98	78.15
$G_2^{R_2}$	29.34	77.22	56.81	66.79	42.88	57.42	9.72	26.72	73.46	56.65	65.42	41.29	58.02	13.90
$G_3^{R_2}$	28.16	70.87	62.42	63.99	42.15	55.86	8.51	25.87	75.32	52.59	64.33	38.39	56.13	13.10
$G_4^{R_2}$	21.06	31.74	43.10	61.34	41.97	40.42	4.16	23.75	43.72	52.74	61.23	47.02	48.98	9.59
$G_5^{R_2}$	94.48	87.82	87.93	67.98	63.94	75.11	70.27	93.95	88.18	89.25	69.48	62.43	77.77	63.84
$G_6^{R_2}$	92.88	84.21	60.11	56.88	26.22	55.48	53.53	94.58	88.53	67.47	67.19	29.53	58.16	81.63
$G_7^{R_2}$	94.74	86.64	68.53	57.90	42.65	67.65	68.04	94.91	79.53	82.50	64.53	46.21	67.11	79.01
R_1	86.74	88.55	81.41	64.00	59.07	40.37	24.95	91.76	91.35	74.89	67.30	56.15	48.60	67.28
R_2	94.86	90.12	91.09	77.14	70.84	77.67	68.05	93.55	89.51	81.34	80.61	61.38	79.93	74.14
$R = [R_1, R_2]$	94.20	91.49	93.10	86.00	78.37	83.13	60.42	95.60	96.15	93.14	89.26	78.78	83.36	82.45

Table 9. The *F*-score of the individual RFs using optical features.

	Balanced							Imbalanced						
	Corn	Peas	Canola	Soybeans	Oats	Wheat	Broadleaf	Corn	Peas	Canola	Soybeans	Oats	Wheat	Broadleaf
$G_1^{O_1}$	40.44	55.71	96.33	61.24	60.17	69.06	21.23	47.90	73.39	98.45	69.29	53.35	71.46	52.18
$G_2^{O_1}$	30.97	45.24	92.98	64.04	48.67	70.65	14.60	30.99	72.52	97.80	65.47	48.83	74.49	36.02
$G_3^{O_1}$	57.73	51.51	96.15	77.22	58.50	69.71	37.99	58.42	84.99	98.10	79.77	51.33	70.05	51.20
$G_4^{O_1}$	26.72	10.06	70.55	62.97	24.41	54.03	18.14	24.03	12.56	84.36	72.43	28.36	59.34	23.50
$G_5^{O_1}$	21.46	10.47	56.21	32.41	29.84	59.17	6.70	33.98	4.98	52.07	34.45	31.01	65.14	11.99
$G_1^{O_2}$	84.18	60.97	98.78	69.50	54.87	71.69	8.72	72.46	90.25	97.98	76.01	52.02	82.80	50.14
$G_2^{O_2}$	47.22	23.17	78.33	35.30	24.04	40.84	2.99	55.75	57.04	94.74	41.73	33.46	49.85	6.29
$G_3^{O_2}$	78.77	56.90	76.21	52.05	37.15	52.55	2.51	76.32	91.91	94.89	63.24	48.94	68.53	13.70
$G_4^{O_2}$	32.25	40.08	74.04	44.45	14.27	53.37	11.99	28.97	53.82	75.45	49.30	16.68	62.40	13.49
$G_5^{O_2}$	61.16	6.53	78.62	15.55	13.55	18.69	3.61	44.09	4.09	74.60	33.62	10.87	39.68	10.63
O_1	45.00	68.39	97.08	70.39	61.26	70.94	44.51	50.08	85.11	98.49	74.53	52.81	69.73	54.94
O_2	83.54	89.42	97.53	70.60	53.28	71.47	25.33	73.21	98.34	98.37	77.01	58.20	81.14	49.33
$O = [O_1, O_2]$	79.30	62.45	97.91	86.48	70.10	78.78	42.12	90.81	71.85	98.93	94.11	60.37	80.24	79.11

Table 10. The *F*-score of the individual RFs using combination of optical and radar features.

		Corn	Peas	Canola	Soybeans	Oats	Wheat	Broadleaf
R_1O_1 = [R_1, O_1]	Balanced	92.81	91.47	96.34	86.34	73.04	79.49	36.76
	Imbalanced	94.92	94.52	98.49	87.89	79.21	82.60	86.96
R_2O_2 = [R_2, O_2]	Balanced	95.79	91.17	98.46	82.39	73.22	77.85	70.72
	Imbalanced	95.32	96.43	98.48	84.96	75.02	84.69	82.10
RO = [R, O]	Balanced	93.17	89.85	97.57	90.11	75.57	84.39	59.76
	Imbalanced	93.77	95.44	98.76	92.65	80.48	89.75	83.32

Table 11. The *F*-score of the traditional and the proposed stacking methods.

		Corn	Peas	Canola	Soybeans	Oats	Wheat	Broadleaf
Traditional Stacking	Balanced	93.30	96.91	95.14	83.45	79.38	76.01	80.76
	Imbalanced	69.53	92.41	93.00	83.82	79.32	83.38	30.97
Strategy 1: G × OA	Balanced	95.22	94.37	98.52	90.94	79.83	86.08	64.61
	Imbalanced	96.47	96.74	99.04	96.94	89.20	93.92	86.35
Strategy 2: HIF × SC	Balanced	95.23	87.99	98.64	92.95	78.29	85.80	71.41
	Imbalanced	96.28	96.89	99.25	96.48	85.59	91.79	88.00
Strategy 3: MSF × J	Balanced	95.61	88.21	98.77	92.86	78.39	85.76	74.46
	Imbalanced	96.68	96.98	99.37	96.39	85.09	91.58	87.68

Table 12. The results of McNemar's test between the traditional and the proposed stacking methods.

Pairwise comparison		$\|z\|$ value	Significance
Strategy 1 vs. traditional stacking	Balanced	15.13	Yes
	Imbalanced	11.78	Yes
Strategy 2 vs. traditional stacking	Balanced	8.42	Yes
	Imbalanced	9.63	Yes
Strategy 3 vs. traditional stacking	Balanced	8.11	Yes
	Imbalanced	10.71	Yes

5.5. Improving proposed methods

Table 4 to 11 show that the proposed strategies, despite higher capability than all the methods, were unable to achieve standard accuracy for all the crop types with the 5% balanced training samples. Due to the difficulties and limitations of sample collection for classification, researchers are usually eager to use balanced training samples. This issue prompted us to conduct more experiments with larger balanced training set sizes. After several experiments, we were finally able to achieve *F*-score accuracy higher than 85% for all the crop types with the 15% balanced training samples and when nTrees = 10. This result was very promising, thanks to its lower cost. The reasons were as follows. Firstly, the ratio of training samples was 1 to 13.6, compared to the 5% of imbalanced training samples. Secondly, the number of trees decreased by 50 times compared to before. Thirdly, the classification process was up to 13 times faster (see Figure 7). The OA values also reached up to 93%. The classification maps of the proposed strategies with these balanced training data (Figure 8), similar to the maps with the 5% imbalanced training data (Figure 6(b)(ii), (c)(ii), and (d)(ii)), were homogeneous and uniform. In particular, the confusion of wheat and oat was much less than before.

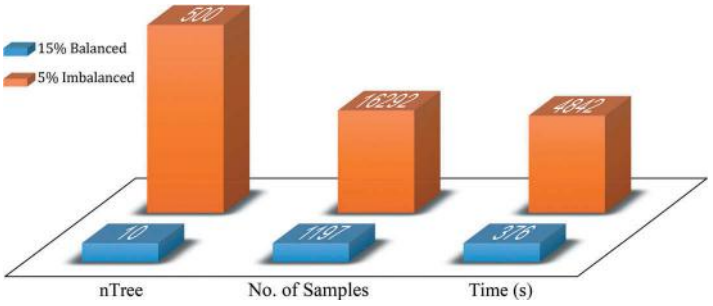

Figure 7. Comparison of two high-accuracy classification tasks with the 15% balanced and the 5% imbalanced training samples.

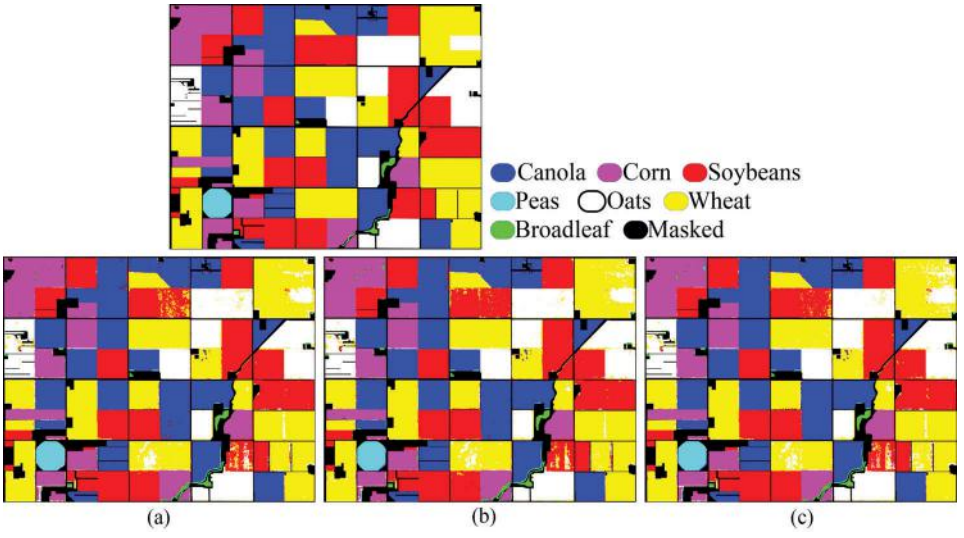

Figure 8. Classification maps of the proposed stacking methods with the 15% balanced training samples: (a) Strategy 1: G× OA, (b) Strategy 2: HIF×SC, and (c) Strategy 3: MSF×J.

6. Conclusion

Crop mapping from bi-temporal optical RapidEye and PolSAR UAVSAR imagery was the focus of this research. A decision fusion framework, based on the RF classifier, was established, which explored and efficiently utilized a diverse set of spectral, textural and polarimetric features for the classification of certain crop types, such as corn, canola, peas, soybeans, oat and wheat in the study area of the SMAPVEX 2012 campaign. Three stacked generalization methods based on an additional RF were proposed in this paper.

We observed that none of the radar and optical features and their combinations and even, traditional stacking method could achieve standard accuracy (*F*-score ≥85%) for all the crop types. The classification maps of the radar features usually mixed up soybeans with canola or wheat. By contrast, the classification maps of the optical features naturally mixed up wheat and oat, as well as soybeans and peas. On the maps involving the combination of both, there were some mixed pixels of soybeans, wheat and oat

together. In addition, the maps of the traditional stacking method mixed up soybeans with corn, canola, and wheat or oats.

The proposed stacking methods were able to achieve higher OA and κ, as well as standard accuracy for all the crop types with the lowest running cost. We needed only 170 pixels per class and only 10 trees for the RF classifier for this purpose. Moreover, the maps obtained by the proposed methods were more homogeneous and desirable. In general, these maps were more applicable to agricultural organizations. Moreover, the problems of mixed pixels of wheat and oat, wheat and soybeans, and oat and soybeans were significantly and efficiently resolved by these maps. It's noteworthy that all these achievements were gained without any advanced object-based image analysis. Furthermore, the proposed methods had lower sensitivity and higher stability to data distribution than the other methods especially the traditional method.

On the whole, the proposed methodology had an intelligible, communicative and simple structure. Therefore, it can be suggested as suitable for performing operational crop mapping and monitoring on local to national scales, using the freely available optical and radar earth observations facilitated by Sentinel-1 and −2, Landsat 8 and the future RCM.

Acknowledgments

The authors would like to present their acknowledgments to the JPL NASA for the PolSAR images, and the SMAPVEX 2012 team, the Agriculture and Agri-Food Canada, and Dr. S. Homayouni, from the Dept. of Geography, Environment, and Geomatics of the University of Ottawa, Canada, for providing for the PolSAR and the optical and fields survey data used in this research. This research was partially supported by the Iranian National Elites Foundation.

Disclosure statement

No potential conflict of interest was reported by the authors.

References

Alberga, V., G. Satalino, and D. K. Staykova. 2008. "Comparison of Polarimetric SAR Observables in Terms of Classification Performance." *International Journal of Remote Sensing* 29 (14): 4129–4150. doi:10.1080/01431160701840182.

Belgiu, M., and O. Csillik. 2018. "Sentinel-2 Cropland Mapping Using Pixel-Based and Object-Based Time-Weighted Dynamic Time Warping Analysis." *Remote Sensing of Environment* 204: 509–523. doi:10.1016/j.rse.2017.10.005.

Belgiu, M., and L. Drăguţ. 2016. "Random Forest in Remote Sensing: A Review of Applications and Future Directions." *ISPRS Journal of Photogrammetry and Remote Sensing* 114: 24–31. doi:10.1016/j.isprsjprs.2016.01.011.

Benediktsson, J. A., and I. Kanellopoulos. 1999. "Classification of Multisource and Hyperspectral Data Based on Decision Fusion." *IEEE Transactions on Geoscience and Remote Sensing* 37 (3): 1367–1377. doi:10.1109/36.763301.

Bigdeli, B., F. Samadzadegan, and P. Reinartz. 2013. "A Multiple SVM System for Classification of Hyperspectral Remote Sensing Data." *Journal of the Indian Society of Remote Sensing* 41 (4): 763–776. doi:10.1007/s12524-013-0286-z.

Bouvet, A., and T. Le Toan. 2011. "Use of ENVISAT/ASAR Wide-Swath Data for Timely Rice Fields Mapping in the Mekong River Delta." *Remote Sensing of Environment* 115 (4): 1090–1101. doi:10.1016/j.rse.2010.12.014.

Braun, A. C., U. Weidner, and S. Hinz. 2012. "Classification in High-Dimensional Feature spaces—Assessment Using SVM, IVM and RVM with Focus on Simulated EnMAP Data." *IEEE Journal of Selected Topics in Applied Earth Observations and Remote Sensing* 5 (2): 436–443. doi:10.1109/JSTARS.2012.2190266.

Breiman, L. 1996. "Bagging Predictors." *Machine Learning* 24 (2): 123–140. doi:10.1007/BF00058655.

Breiman, L. 2001. "Random Forests." *Machine Learning* 45 (1): 5–32. doi:10.1023/A:1010933404324.

Brisco, B., K. Li, B. Tedford, F. Charbonneau, S. Yun, and K. Murnaghan. 2013. "Compact Polarimetry Assessment for Rice and Wetland Mapping." *International Journal of Remote Sensing* 34 (6): 1949–1964. doi:10.1080/01431161.2012.730156.

Canisius, F., J. Shang, J. Liu, X. Huang, B. Ma, X. Jiao, X. Geng, J. M. Kovacs, and D. Walters. 2018. "Tracking Crop Phenological Development Using Multi-Temporal Polarimetric Radarsat-2 Data." *Remote Sensing of Environment* 210: 508–518. doi:10.1016/j.rse.2017.07.031.

Ceamanos, X., B. Waske, J. A. Benediktsson, J. Chanussot, M. Fauvel, and J. R. Sveinsson. 2010. "A Classifier Ensemble Based on Fusion of Support Vector Machines for Classifying Hyperspectral Data." *International Journal of Image and Data Fusion* 1 (4): 293–307. doi:10.1080/19479832.2010.485935.

Chellasamy, M., R. T. Zielinski, and M. H. Greve. 2014. "A Multievidence Approach for Crop Discrimination Using Multitemporal WorldView-2 Imagery." *IEEE Journal of Selected Topics in Applied Earth Observations and Remote Sensing* 7 (8): 3491–3501. doi:10.1109/JSTARS.2014.2349945.

Chen, C. F., N. T. Son, L. Y. Chang, and C. R. Chen. 2011. "Classification of Rice Cropping Systems by Empirical Mode Decomposition and Linear Mixture Model for Time-Series MODIS 250 M NDVI Data in the Mekong Delta, Vietnam." *International Journal of Remote Sensing* 32 (18): 5115–5134. doi:10.1080/01431161.2010.494639.

Chen, J., C. Wang, and R. Wang. 2009. "Using Stacked Generalization to Combine SVMs in Magnitude and Shape Feature Spaces for Classification of Hyperspectral Data." *IEEE Transactions on Geoscience and Remote Sensing* 47 (7): 2193–2205. doi:10.1109/TGRS.2008.2010491.

Clevers, J. G., L. Kooistra, and M. M. M. van Den Brande. 2017. "Using Sentinel-2 Data for Retrieving LAI and Leaf and Canopy Chlorophyll Content of a Potato Crop." *Remote Sensing* 9 (5): 405. doi:10.3390/rs9050405.

Cloude, S. R., and E. Pottier. 1996. "A Review of Target Decomposition Theorems in Radar Polarimetry." *IEEE Transactions on Geoscience and Remote Sensing* 34 (2): 498–518. doi:10.1109/36.485127.

Cloude, S. R., and E. Pottier. 1997. "An Entropy Based Classification Scheme for Land Applications of Polarimetric SAR." *IEEE Transactions on Geoscience and Remote Sensing* 35 (1): 68–78. doi:10.1109/36.551935.

Congalton, R. G. 1991. "A Review of Assessing the Accuracy of Classifications of Remotely Sensed Data." *Remote Sensing of Environment* 37 (1): 35–46. doi:10.1016/0034-4257(91)90048-B.

Cunningham, P., J. Carney, and S. Jacob. 2000. "Stability Problems with Artificial Neural Networks and the Ensemble Solution." *Artificial Intelligence in Medicine* 20 (3): 217–225.

Denize, J., L. Hubert-Moy, J. Betbeder, S. Corgne, J. Baudry, and E. Pottier. 2019. "Evaluation of Using Sentinel-1 And-2 Time-Series to Identify Winter Land Use in Agricultural Landscapes." *Remote Sensing* 11 (1): 37. doi:10.3390/rs11010037.

Du, P., J. Xia, W. Zhang, K. Tan, Y. Liu, and S. Liu. 2012. "Multiple Classifier System for Remote Sensing Image Classification: A Review." *Sensors* 12 (4): 4764–4792. doi:10.3390/s120404764.

Dubois, P. C., J. Van Zyl, and T. Engman. 1995. "Measuring Soil Moisture with Imaging Radars." *IEEE Transactions on Geoscience and Remote Sensing* 33 (4): 915–926. doi:10.1109/36.406677.

Eisavi, V., S. Homayouni, and E. Rezaei-Chiyaneh. 2017. "Apple Orchard Phenology Response to Desiccation and Temperature Changes in Urmia Lake Region." *International Journal of Environmental Science and Technology* 14 (9): 1865–1878. doi:10.1007/s13762-017-1283-5.

Entezari, I., M. Motagh, and B. Mansouri. 2012. "Comparison of the Performance of L-Band Polarimetric Parameters for Land Cover Classification." *Canadian Journal of Remote Sensing* 38 (5): 629–643. doi:10.5589/m12-051.

Esch, T., A. Metz, M. Marconcini, and M. Keil. 2014. "Combined Use of Multi-Seasonal High and Medium Resolution Satellite Imagery for Parcel-Related Mapping of Cropland and Grassland."

International Journal of Applied Earth Observation and Geoinformation 28: 230–237. doi:10.1016/j.jag.2013.12.007.

Ferrant, S., A. Selles, M. Le Page, P. A. Herrault, C. Pelletier, A. Al-Bitar, S. Mermoz, et al. 2017. "Detection of Irrigated Crops from Sentinel-1 and Sentinel-2 Data to Estimate Seasonal Groundwater Use in South India." *Remote Sensing* 9 (11): 1119. doi:10.3390/rs9111119.

Forkuor, G., C. Conrad, M. Thiel, T. Ullmann, and E. Zoungrana. 2014. "Integration of Optical and Synthetic Aperture Radar Imagery for Improving Crop Mapping in Northwestern Benin, West Africa." *Remote Sensing* 6 (7): 6472–6499. doi:10.3390/rs6076472.

Freeman, A., and S. L. Durden. 1998. "A Three-Component Scattering Model for Polarimetric SAR Data." *IEEE Transactions on Geoscience and Remote Sensing* 36 (3): 963–973. doi:10.1109/36.673687.

Gonzalez, R. C., and R. E. Woods. 2002. Digital Image Processing. 2nd Edition, Prentice Hall, Upper Saddle River.

Guo, B., S. R. Gunn, R. I. Damper, and J. D. Nelson. 2006. "Band Selection for Hyperspectral Image Classification Using Mutual Information." *IEEE Geoscience and Remote Sensing Letters* 3 (4): 522–526. doi:10.1109/LGRS.2006.878240.

Haboudane, D., J. R. Miller, E. Pattey, P. J. Zarco-Tejada, and I. B. Strachan. 2004. "Hyperspectral Vegetation Indices and Novel Algorithms for Predicting Green LAI of Crop Canopies: Modeling and Validation in the Context of Precision Agriculture." *Remote Sensing of Environment* 90 (3): 337–352. doi:10.1016/j.rse.2003.12.013.

Haldar, D., C. Patnaik, S. Mohan, and M. Chakraborty. 2012. "Jute and Tea Discrimination through Fusion of SAR and Optical Data." *Progress In Electromagnetics Research* 39: 337–354. doi:10.2528/PIERB11123011.

Haralick, R. M., and K. Shanmugam. 1973. "Textural Features for Image Classification." *IEEE Transactions on Systems, Man, and Cybernetics* 3 (6): 610–621. doi:10.1109/TSMC.1973.4309314.

Hoang, H. K., M. Bernier, S. Duchesne, and Y. M. Tran. 2016. "Rice Mapping Using Radarsat-2 Dual-And Quad-Pol Data in a Complex Land-Use Watershed: Cau River Basin (Vietnam)." *IEEE Journal of Selected Topics in Applied Earth Observations and Remote Sensing* 9 (7): 3082–3096. doi:10.1109/JSTARS.2016.2586102.

Hoekman, D. H., M. A. Vissers, and T. N. Tran. 2011. "Unsupervised Full-Polarimetric SAR Data Segmentation as a Tool for Classification of Agricultural Areas." *IEEE Journal of Selected Topics in Applied Earth Observations and Remote Sensing* 4 (2): 402–411. doi:10.1109/JSTARS.2010.2042280.

Hosseini, M., H. McNairn, A. Merzouki, and A. Pacheco. 2015. "Estimation of Leaf Area Index (LAI) in Corn and Soybeans Using Multi-Polarization C- and L-Band Radar Data." *Remote Sensing of Environment* 170: 77–89. doi:10.1016/j.rse.2015.09.002.

Hütt, C., W. Koppe, Y. Miao, and G. Bareth. 2016. "Best Accuracy Land Use/Land Cover (LULC) Classification to Derive Crop Types Using Multitemporal, Multisensor, and Multi-Polarization SAR Satellite Images." *Remote Sensing* 8 (8): 684. doi:10.3390/rs8080684.

Immitzer, M., F. Vuolo, and C. Atzberger. 2016. "First Experience with Sentinel-2 Data for Crop and Tree Species Classifications in Central Europe." *Remote Sensing* 8 (3): 166. doi:10.3390/rs8030166.

Inglada, J., A. Vincent, M. Arias, and C. Marais-Sicre. 2016. "Improved Early Crop Type Identification by Joint Use of High Temporal Resolution SAR and Optical Image Time Series." *Remote Sensing* 8 (5): 362. doi:10.3390/rs8050362.

James, G., D. Witten, T. Hastie, and R. Tibshirani. 2013. *An Introduction to Statistical Learning*, 316–321. Vol. 6. New York: springer.

Jiao, X., J. M. Kovacs, J. Shang, H. McNairn, D. Walters, B. Ma, and X. Geng. 2014. "Object-Oriented Crop Mapping and Monitoring Using Multi-Temporal Polarimetric Radarsat-2 Data." *ISPRS Journal of Photogrammetry and Remote Sensing* 96: 38–46. doi:10.1016/j.isprsjprs.2014.06.014.

Jin, X., J. Ma, Z. Wen, and K. Song. 2015. "Estimation of Maize Residue Cover Using Landsat-8 OLI Image Spectral Information and Textural Features." *Remote Sensing* 7 (11): 14559–14575. doi:10.3390/rs71114559.

Joshi, N., M. Baumann, A. Ehammer, R. Fensholt, K. Grogan, P. Hostert, M. R. Jepsen, et al. 2016. "A Review of the Application of Optical and Radar Remote Sensing Data Fusion to Land Use Mapping and Monitoring." *Remote Sensing* 8 (1): 1–23. doi:10.3390/rs8010070.

Khosravi, I., A. Safari, S. Homayouni, and H. McNairn. 2017. "Enhanced Decision Tree Ensembles for Land-Cover Mapping from Fully Polarimetric SAR Data." *International Journal of Remote Sensing* 38 (23): 7138–7160. doi:10.1080/01431161.2017.1372863.

Kim, H. O., and J. M. Yeom. 2014. "Effect of Red-Edge and Texture Features for Object-Based Paddy Rice Crop Classification Using RapidEye Multi-Spectral Satellite Image Data." *International Journal of Remote Sensing* 35 (19): 7046–7068.

Krogager, E. 1990. "New Decomposition of the Radar Target Scattering Matrix." *Electronics Letters* 26 (18): 1525–1527. doi:10.1049/el:19900979.

Kross, A., H. McNairn, D. Lapen, M. Sunohara, and C. Champagne. 2015. "Assessment of RapidEye Vegetation Indices for Estimation of Leaf Area Index and Biomass in Corn and Soybean Crops." *International Journal of Applied Earth Observation and Geoinformation* 34: 235–248. doi:10.1016/j.jag.2014.08.002.

Kussul, N., G. Lemoine, F. J. Gallego, S. V. Skakun, M. Lavreniuk, and A. Y. Shelestov. 2016. "Parcel-Based Crop Classification in Ukraine Using Landsat-8 Data and Sentinel-1A Data." *IEEE Journal of Selected Topics in Applied Earth Observations and Remote Sensing* 9 (6): 2500–2508. doi:10.1109/JSTARS.2016.2560141.

Lardeux, C., P. L. Frison, C. Tison, J. C. Souyris, B. Stoll, B. Fruneau, and J. P. Rudant. 2009. "Support Vector Machine for Multifrequency SAR Polarimetric Data Classification." *IEEE Transactions on Geoscience and Remote Sensing* 47 (12): 4143–4152. doi:10.1109/TGRS.2009.2023908.

Larrañaga, A., and J. Álvarez-Mozos. 2016. "On the Added Value of Quad-Pol Data in a Multi-Temporal Crop Classification Framework Based on Radarsat-2 Imagery." *Remote Sensing* 8 (4): 335. doi:10.3390/rs8040335.

Larrañaga, A., J. Álvarez-Mozos, and L. Albizua. 2011. "Crop Classification in Rain-Fed and Irrigated Agricultural Areas Using Landsat TM and ALOS/PALSAR Data." *Canadian Journal of Remote Sensing* 37 (1): 157–170. doi:10.5589/m11-022.

Lee, J. S., and E. Pottier. 2009. *Polarimetric Radar Imaging: From Basics to Applications*. Boca Raton, FL: CRC press. doi:10.1201/9781420054989.

Liu, C., J. Shang, P. W. Vachon, and H. McNairn. 2013. "Multiyear Crop Monitoring Using Polarimetric Radarsat-2 Data." *IEEE Transactions on Geoscience and Remote Sensing* 51 (4): 2227–2240. doi:10.1109/TGRS.2012.2208649.

Löw, F., G. Schorcht, U. Michel, S. Dech, and C. Conrad. 2012. "Per-Field Crop Classification in Irrigated Agricultural Regions in Middle Asia Using Random Forest and Support Vector Machine Ensemble. In SPIE Remote Sensing." In *International Society for Optics and Photonics*, 85380R–85380R.

Mansaray, L. R., W. Huang, D. Zhang, J. Huang, and J. Li. 2017. "Mapping Rice Fields in Urban Shanghai, Southeast China, Using Sentinel-1A and Landsat 8 Datasets." *Remote Sensing* 9 (3): 257. doi:10.3390/rs9030257.

Martinez-Uso, A., F. Pla, J. M. Sotoca, and P. Garcia-Sevilla (2006, August). "Clustering-Based Multispectral Band Selection Using Mutual Information." *In Pattern* Recognition, *2006. ICPR 2006. 18th International Conference on* (Vol. 2, pp. 760–763). IEEE.

McNairn, H., C. Champagne, J. Shang, D. Holmstrom, and G. Reichert. 2009a. "Integration of Optical and Synthetic Aperture Radar (SAR) Imagery for Delivering Operational Annual Crop Inventories." *ISPRS Journal of Photogrammetry and Remote Sensing* 64 (5): 434–449. doi:10.1016/j.isprsjprs.2008.07.006.

McNairn, H., T. J. Jackson, G. Wiseman, S. Bélair, A. A. Berg, P. R. Bullock, A. Colliander, et al. 2015. "The Soil Moisture Active Passive Validation Experiment 2012 (SMAPVEX12): Prelaunch Calibration and Validation of the SMAP Soil Moisture Algorithms." *IEEE Transactions on Geoscience and Remote Sensing* 53 (5): 2784–2801. doi:10.1109/TGRS.2014.2364913.

McNairn, H., J. Shang, X. Jiao, and C. Champagne. 2009b. "The Contribution of ALOS PALSAR Multipolarization and Polarimetric Data to Crop Classification." *IEEE Transactions on Geoscience and Remote Sensing* 47 (12): 3981–3992. doi:10.1109/TGRS.2009.2026052.

Mountrakis, G., J. Im, and C. Ogole. 2011. "Support Vector Machines in Remote Sensing: A Review." *ISPRS Journal of Photogrammetry and Remote Sensing* 66 (3): 247–259. doi:10.1016/j.isprsjprs.2010.11.001.

Navarro, A., J. Rolim, I. Miguel, J. Catalão, J. Silva, M. Painho, and Z. Vekerdy. 2016. "Crop Monitoring Based on SPOT-5 Take-5 and Sentinel-1A Data for the Estimation of Crop Water Requirements." *Remote Sensing* 8 (6): 525. doi:10.3390/rs8060525.

Ng, W. T., P. Rima, K. Einzmann, M. Immitzer, C. Atzberger, and S. Eckert. 2017. "Assessing the Potential of Sentinel-2 and Pléiades Data for the Detection of Prosopis and Vachellia Spp. In Kenya." *Remote Sensing* 9 (1): 74. doi:10.3390/rs9010074.

Niu, X., and Y. Ban. 2013. "Multitemporal Polarimetric Radarsat-2 SAR Data for Urban Land Cover Mapping through a Dictionary-Based and a Rule-Based Model Selection in a Contextual SEM Algorithm." *Canadian Journal of Remote Sensing* 39 (2): 138–151. doi:10.5589/m13-019.

Panigrahy, S., V. Jain, C. Patnaik, and J. S. Parihar. 2012. "Identification of Aman Rice Crop in Bangladesh Using Temporal C-Band SAR–A Feasibility Study." *Journal of the Indian Society of Remote Sensing* 40 (4): 599–606. doi:10.1007/s12524-011-0193-0.

Peña, M. A., and A. Brenning. 2015. "Assessing Fruit-Tree Crop Classification from Landsat-8 Time Series for the Maipo Valley, Chile." *Remote Sensing of Environment* 171: 234–244. doi:10.1016/j.rse.2015.10.029.

Peña-Barragán, J. M., M. K. Ngugi, R. E. Plant, and J. Six. 2011. "Object-Based Crop Identification Using Multiple Vegetation Indices, Textural Features and Crop Phenology." *Remote Sensing of Environment* 115 (6): 1301–1316. doi:10.1016/j.rse.2011.01.009.

Pittman, K., M. C. Hansen, I. Becker-Reshef, P. V. Potapov, and C. O. Justice. 2010. "Estimating Global Cropland Extent with Multi-Year MODIS Data." *Remote Sensing* 2 (7): 1844–1863. doi:10.3390/rs2071844.

Polikar, R. 2006. "Ensemble Based Systems in Decision Making." *IEEE Circuits and Systems Magazine* 6 (3): 21–45. doi:10.1109/MCAS.2006.1688199.

Powers, D. M. (2011). Evaluation: from precision, recall and F-measure to ROC, informedness, markedness and correlation.

Qi, Z., A. G. O. Yeh, X. Li, and Z. Lin. 2012. "A Novel Algorithm for Land Use and Land Cover Classification Using Radarsat-2 Polarimetric SAR Data." *Remote Sensing of Environment* 118: 21–39. doi:10.1016/j.rse.2011.11.001.

Qiao, C., B. Daneshfar, and A. M. Davidson. 2017. "The Application of Discriminant Analysis for Mapping Cereals and Pasture Using Object-Based Features." *International Journal of Remote Sensing* 38 (20): 5546–5568. doi:10.1080/01431161.2017.1325530.

Rignot, E. J., S. J. Ostro, J. J. van Zyl, and K. C. Jezek. 1993. "Unusual Radar Echoes from the Greenland Ice Sheet." *Science* 261: 1710–1713. doi:10.1126/science.261.5129.1710.

Rodriguez-Galiano, V. F., B. Ghimire, J. Rogan, M. Chica-Olmo, and J. P. Rigol-Sanchez. 2012. "An Assessment of the Effectiveness of a Random Forest Classifier for Land-Cover Classification." *ISPRS Journal of Photogrammetry and Remote Sensing* 67: 93–104. doi:10.1016/j.isprsjprs.2011.11.002.

Roosjen, P. P., J. M. Suomalainen, H. M. Bartholomeus, and J. G. Clevers. 2016. "Hyperspectral Reflectance Anisotropy Measurements Using a Pushbroom Spectrometer on an Unmanned Aerial vehicle—Results for Barley, Winter Wheat, and Potato." *Remote Sensing* 8 (11): 909. doi:10.3390/rs8110909.

Salehi, B., B. Daneshfar, and A. M. Davidson. 2017. "Accurate Crop-Type Classification Using Multi-Temporal Optical and Multi-Polarization SAR Data in an Object-Based Image Analysis Framework." *International Journal of Remote Sensing* 38 (14): 4130–4155. doi:10.1080/01431161.2017.1317933.

Samadzadegan, F., and E. Ferdosi. 2012. "Classification of Polarimetric SAR Images Based on Optimum SVMs Classifier Using Bees Algorithm." *Polarization* 6: 9.

Schultz, B., M. Immitzer, A. R. Formaggio, I. D. A. Sanches, A. J. B. Luiz, and C. Atzberger. 2015. "Self-Guided Segmentation and Classification of Multi-Temporal Landsat 8 Images for Crop Type Mapping in Southeastern Brazil." *Remote Sensing* 7 (11): 14482–14508. doi:10.3390/rs71114482.

Schuster, C., M. Förster, and B. Kleinschmit. 2012. "Testing the Red Edge Channel for Improving Land-Use Classifications Based on High-Resolution Multi-Spectral Satellite Data." *International Journal of Remote Sensing* 33 (17): 5583–5599. doi:10.1080/01431161.2012.666812.

Siachalou, S., G. Mallinis, and M. Tsakiri-Strati. 2015. "A Hidden Markov Models Approach for Crop Classification: Linking Crop Phenology to Time Series of Multi-Sensor Remote Sensing Data." *Remote Sensing* 7 (4): 3633–3650. doi:10.3390/rs70403633.

Skakun, S., N. Kussul, A. Y. Shelestov, M. Lavreniuk, and O. Kussul. 2016. "Efficiency Assessment of Multitemporal C-Band Radarsat-2 Intensity and Landsat-8 Surface Reflectance Satellite Imagery

for Crop Classification in Ukraine." *IEEE Journal of Selected Topics in Applied Earth Observations and Remote Sensing* 9 (8): 3712–3719. doi:10.1109/JSTARS.2015.2454297.

Son, N. T., C. F. Chen, C. R. Chen, H. N. Duc, and L. Y. Chang. 2014. "A Phenology-Based Classification of Time-Series MODIS Data for Rice Crop Monitoring in Mekong Delta, Vietnam." *Remote Sensing* 6 (1): 135–156. doi:10.3390/rs6010135.

Song, X., C. Yang, M. Wu, C. Zhao, G. Yang, W. C. Hoffmann, and W. Huang. 2017. "Evaluation of Sentinel-2A Satellite Imagery for Mapping Cotton Root Rot." *Remote Sensing* 9 (9): 906. doi:10.3390/rs9090906.

Sonobe, R., Y. Yamaya, H. Tani, X. Wang, N. Kobayashi, and K. I. Mochizuki. 2017. "Mapping Crop Cover Using Multi-Temporal Landsat 8 OLI Imagery." *International Journal of Remote Sensing* 38 (15): 4348–4361. doi:10.1080/01431161.2017.1323286.

Steinhausen, M. J., P. D. Wagner, B. Narasimhan, and B. Waske. 2018. "Combining Sentinel-1 and Sentinel-2 Data for Improved Land Use and Land Cover Mapping of Monsoon Regions." *International Journal of Applied Earth Observation and Geoinformation* 73: 595–604. doi:10.1016/j.jag.2018.08.011.

Tamiminia, H., S. Homayouni, H. McNairn, and A. Safari. 2017. "A Particle Swarm Optimized Kernel-Based Clustering Method for Crop Mapping from Multi-Temporal Polarimetric L-Band SAR Observations." *International Journal of Applied Earth Observation and Geoinformation* 58: 201–212. doi:10.1016/j.jag.2017.02.010.

Theodoridis, S., and K. Koutroumbas. 2003. *Pattern Recognition*. 2nd ed. New York, NY: Academic Press.

Torbick, N., D. Chowdhury, W. Salas, and J. Qi. 2017. "Monitoring Rice Agriculture across Myanmar Using Time Series Sentinel-1 Assisted by Landsat-8 and PALSAR-2." *Remote Sensing* 9 (2): 119. doi:10.3390/rs9020119.

Torbick, N., W. A. Salas, S. Hagen, and X. Xiao. 2011. "Monitoring Rice Agriculture in the Sacramento Valley, USA with Multitemporal PALSAR and MODIS Imagery." *IEEE Journal of Selected Topics in Applied Earth Observations and Remote Sensing* 4 (2): 451–457. doi:10.1109/JSTARS.2010.2091493.

Ursani, A. A., K. Kpalma, C. C. Lelong, and J. Ronsin. 2012. "Fusion of Textural and Spectral Information for Tree Crop and Other Agricultural Cover Mapping with Very-High Resolution Satellite Images." *IEEE Journal of Selected Topics in Applied Earth Observations and Remote Sensing* 5 (1): 225–235. doi:10.1109/JSTARS.2011.2170289.

Van Tricht, K., A. Gobin, S. Gilliams, and I. Piccard. 2018. "Synergistic Use of Radar Sentinel-1 and Optical Sentinel-2 Imagery for Crop Mapping: A Case Study for Belgium." *Remote Sensing* 10 (10): 1642. doi:10.3390/rs10101642.

Villa, P., D. Stroppiana, G. Fontanelli, R. Azar, and P. A. Brivio. 2015. "In-Season Mapping of Crop Type with Optical and X-Band SAR Data: A Classification Tree Approach Using Synoptic Seasonal Features." *Remote Sensing* 7 (10): 12859–12886. doi:10.3390/rs71012859.

Vintrou, E., A. Desbrosse, A. Bégué, S. Traoré, C. Baron, and D. L. Seen. 2012. "Crop Area Mapping in West Africa Using Landscape Stratification of MODIS Time Series and Comparison with Existing Global Land Products." *International Journal of Applied Earth Observation and Geoinformation* 14 (1): 83–93. doi:10.1016/j.jag.2011.06.010.

Wang, X. Y., Y. G. Guo, J. He, and L. T. Du. 2016. "Fusion of HJ1B and ALOS PALSAR Data for Land Cover Classification Using Machine Learning Methods." *International Journal of Applied Earth Observation and Geoinformation* 52: 192–203. doi:10.1016/j.jag.2016.06.014.

Wardlow, B. D., and S. L. Egbert. 2010. "A Comparison of MODIS 250-M EVI and NDVI Data for Crop Mapping: A Case Study for Southwest Kansas." *International Journal of Remote Sensing* 31 (3): 805–830. doi:10.1080/01431160902897858.

Waske, B., and J. A. Benediktsson. 2007. "Fusion of Support Vector Machines for Classification of Multisensor Data." *IEEE Transactions on Geoscience and Remote Sensing* 45 (12): 3858–3866. doi:10.1109/TGRS.2007.898446.

Waske, B., and S. van der Linden. 2008. "Classifying Multilevel Imagery from SAR and Optical Sensors by Decision Fusion." *IEEE Transactions on Geoscience and Remote Sensing* 46 (5): 1457–1466. doi:10.1109/TGRS.2008.916089.

Whelen, T., and P. Siqueira. 2017. "Use of Time-Series L-Band UAVSAR Data for the Classification of Agricultural Fields in the San Joaquin Valley." *Remote Sensing of Environment* 193: 216–224. doi:10.1016/j.rse.2017.03.014.

Wolpert, D. H. 1992. "Stacked Generalization." *Neural Networks* 5 (2): 241–259. doi:10.1016/S0893-6080(05)80023-1.

Yamaguchi, Y., T. Moriyama, M. Ishido, and H. Yamada. 2005. "Four-Component Scattering Model for Polarimetric SAR Image Decomposition." *IEEE Transactions on Geoscience and Remote Sensing* 43 (8): 1699–1706. doi:10.1109/TGRS.2005.852084.

You, J., Z. Pei, and D. Wang. 2014. "Crop Mapping of Complex Agricultural Landscapes Based on Discriminant Space." *IEEE Journal of Selected Topics in Applied Earth Observations and Remote Sensing* 7 (11): 4356–4367. doi:10.1109/JSTARS.2014.2320156.

You, X., J. Meng, M. Zhang, and T. Dong. 2013. "Remote Sensing Based Detection of Crop Phenology for Agricultural Zones in China Using a New Threshold Method." *Remote Sensing* 5 (7): 3190–3211. doi:10.3390/rs5073190.

Zhang, H., H. Lin, and Y. Li. 2015. "Impacts of Feature Normalization on Optical and SAR Data Fusion for Land Use/Land Cover Classification." *IEEE Geoscience and Remote Sensing Letters* 12 (5): 1061–1065. doi:10.1109/LGRS.2014.2377722.

Zhang, X., Y. Sun, K. Shang, L. Zhang, and S. Wang. 2016. "Crop Classification Based on Feature Band Set Construction and Object-Oriented Approach Using Hyperspectral Images." *IEEE Journal of Selected Topics in Applied Earth Observations and Remote Sensing* 9 (9): 4117–4128. doi:10.1109/JSTARS.2016.2577339.

Zheng, B., J. B. Campbell, and K. M. de Beurs. 2012. "Remote Sensing of Crop Residue Cover Using Multi-Temporal Landsat Imagery." *Remote Sensing of Environment* 117: 177–183. doi:10.1016/j.rse.2011.09.016.

Zheng, B., S. W. Myint, P. S. Thenkabail, and R. M. Aggarwal. 2015. "A Support Vector Machine to Identify Irrigated Crop Types Using Time-Series Landsat NDVI Data." *International Journal of Applied Earth Observation and Geoinformation* 34: 103–112. doi:10.1016/j.jag.2014.07.002.

Zheng, H., P. Du, J. Chen, J. Xia, E. Li, Z. Xu, X. Li, and N. Yokoya. 2017. "Performance Evaluation of Downscaling Sentinel-2 Imagery for Land Use and Land Cover Classification by Spectral-Spatial Features." *Remote Sensing* 9 (12): 1274. doi:10.3390/rs9121274.

Zhong, B., A. Yang, A. Nie, Y. Yao, H. Zhang, S. Wu, and Q. Liu. 2015. "Finer Resolution Land-Cover Mapping Using Multiple Classifiers and Multisource Remotely Sensed Data in the Heihe River Basin." *IEEE Journal of Selected Topics in Applied Earth Observations and Remote Sensing* 8 (10): 4973–4992. doi:10.1109/JSTARS.2015.2461453.

Zhou, T., J. Pan, P. Zhang, S. Wei, and T. Han. 2017. "Mapping Winter Wheat with Multi-Temporal SAR and Optical Images in an Urban Agricultural Region." *Sensors* 17 (6): 1210. doi:10.3390/s17050968.

Zhu, L., V. C. Radeloff, and A. R. Ives. 2017. "Improving the Mapping of Crop Types in the Midwestern US by Fusing Landsat and MODIS Satellite Data." *International Journal of Applied Earth Observation and Geoinformation* 58: 1–11. doi:10.1016/j.jag.2017.01.012.